Modeling of permafrost temperatures in the Lena River Delta, Siberia, based on remote sensing products

MASTER THESIS

to attain the academic degree

Master of Science (M.Sc.) in Physical Geography

submitted by

Maria Peter

Institute for Geography,

University of Leipzig

Leipzig, December 2014

Maria Peter,

geboren am 25. Oktober 1989 in Berlin

Adresse: Oststraße 6, 04317 Leipzig
email: maria.peter@awi.de
Matrikelnr: 1594759

Erstgutachter: Prof. Dr. Michael Vohland

Adresse: Johannisallee 19a
             Institut für Geographie
             Universität Leipzig
             DE-04103 Leipzig

email: michael.vohland@uni-leipzig.de

Zweitgutachterin: PD Dr. Julia Boike

Adresse: Telegrafenberg A6
             Alfred-Wegener-Institut
             für Polar- und
             Meeresforschung Potsdam
             DE-14473 Potsdam

email: julia.boike@awi.de

ABSTRACT

The northeast Siberian lowlands are a climatically sensitive region dominated by permafrost, but monitoring the thermal ground conditions and predicting its future is challenging for such vast areas. A modeling scheme based on gridded remote sensing data, which was recently published for a single grid cell, was extended to the entire Lena River Delta using the transient permafrost model CryoGrid 2. The model is based on the heat transfer equation, calculating the evolution of the soil temperature for every grid cell. The horizontal grid cell size is determined by the remotely sensed forcing data of MODIS Land Surface Temperature (1x1km) and snow depth (1x1km) that was compiled from the GlobSnow Snow Water Equivalent and MODIS Snow Extent products. To assign subsurface properties for each grid cell, a spatially resolved stratigraphic classification was constructed. Based on field observations, such as studies of vegetation, geomorphology and geology, the Lena River Delta was divided into three stratigraphic classes which differ in their layers and layer characteristics, i.e. the volumetric contents of water/ice, mineral, organic and air. From this soil stratigraphy, the soil thermal properties, such as soil thermal conductivity and volumetric soil heat capacity required for the modeling can be inferred for each depth and grid cell.

A validation of the MODIS LST forcing time series at one point in the delta revealed a cold bias of up to 3 °C when compared to in-situ measured land surface temperatures. When the gaps in the MODIS data series that occurred due to cloud covered scenes were filled with 2 m - air temperature of the ERA-interim reanalysis, the bias was reduced to -0.8 °C in the average. Therefore, the modeling was conducted with this modified temperature forcing.

The model results, in particular ground temperatures and thaw depths, were validated at seven in-situ measurement sites distributed over the delta. For annual average ground temperatures, an agreement within 1°C was found for most validation sites, while modeled and measured thaw depths agreed within 10 cm or less. A sensitivity analysis revealed the influence of the soil stratigraphic classes on ground temperatures and thaw depths, showing differences between classes of more than 2 °C in annual average ground temperature and 50 cm in thaw depths for the same forcing data.

The warmest modeled ground temperatures are calculated for grid cells close to the main river channels in the southern parts of the delta, while the coldest are modeled for the northeastern part, an area with low surface temperatures and snow depths. The lowest thaw depths are modeled for the so-called 'Ice Complex', an area with extremely high ground ice and soil organic contents. The deepest thaw depths are modeled for grid cells which feature low organic and ice contents and no organic upper layer.

The remote sensing driven model scheme demonstrated to be a useful tool for monitoring the thermal state of permafrost and its time evolution in the Lena River Delta. Thus, the approach could be a first step towards operational permafrost monitoring using satellite sensors.

ZUSAMMENFASSUNG

Die vom Permafrost beeinflussten arktischen Tundrenregionen in Nordostsibirien stellen eine der am stärksten vom Klimawandel beeinflussten Landschaften dar. Die Beobachtung und Vorhersage von Tauprozessen des Permafrostes, die mit den heutigen klimatischen Bedingungen und Veränderungen gekoppelt sind, ist für die weiten und schwer erreichbaren Tundrengegenden schwierig. Eine auf Fernerkundungsdaten beruhende Modellierung von Permafrosttemperaturen in unterschiedlichen Bodentiefen wurde bereits für einen Punkt im Lenadelta durchgeführt und validiert (Langer et al. 2013). Diese Berechnungen wurden nun mit einer Grid-Zellengröße von 1x1km auf das gesamte Delta ausgeweitet und mithilfe der Satellitenprodukte MODIS Land Surface Temperature, MODIS Snow Extent und GlobSnow Snow Water Equivalent angetrieben. Nach Validierung des MODIS LST–Produktes mit Messdaten aus der Lena-Delta-Region wurden Lufttemperaturen aus der ERA-interim Reanalyse als Lückenfüller für die MODIS LST Datenreihe genutzt und so eine verbesserte Annährung an die realen Oberflächentemperaturen erzielt. Für die Repräsentation des Bodenaufbaus wurde, basierend auf Literaturrecherche und Schätzungen von mit dem Gebiet vertrauten Wissenschaftlern, eine Stratigraphie für des Modell definiert, die die volumetrischen Gehalte von Wasser/Eis, Organik, mineralischem Anteil und Luftanteil für jede Bodentiefe festlegt. Daraus hervor gingen drei stratigraphische Klassen, die sich in den Ausdehnungen an den drei morphologischen Haupt-Flussterrassen orientieren.

Die Validierung der berechneten Modelldaten erfolgte sowohl für Temperaturen in unterschiedlichen Tiefen als auch für die maximalen Auftautiefen der Böden an sieben verschiedenen Stellen im Delta und auf allen drei Stratigraphieklassen. Für modellierte und gemessene Jahresdurchschnitts-Bodentemperaturen in verschiedenen Tiefen wurde für die meisten Stellen eine Übereinstimmung innerhalb von 1°C berechnet, bei den Auftautiefen belief sich die Genauigkeit zwischen modellierten und berechneten Tiefen auf 10 cm oder weniger. Eine Sensitivitätsanalyse des Modells stellte zudem den großen Einfluss der stratigraphischen Klassifizierung auf die modellierten Bodentemperaturen heraus, besonders auf die Auftautiefen. Für die zweite Klasse der Stratigraphie sind beispielsweise bis zu 2°C höhere Bodentemperaturen und 50 cm größere Auftautiefen berechnet als für die beiden anderen Klassen.

Die wärmsten durchschnittlichen Bodentemperaturen wurden für Grid-Zellen nahe der Hauptflussarme des Deltas berechnet, die kältesten für den nordöstlichen Teil des Deltas und hin zu dessen Küstenlinie, was wahrscheinlich mit niedrigen Schneehöhen im Winter und relativ kalten Oberflächentemperaturen zusammenhängt. Die flachsten Auftautiefen wurden für Zellen der dritten stratigraphischen Klasse und für den nordöstlichen Rand des Modellbereiches berechnet. Die tiefsten wurden für die zweite Stratigraphieklasse berechnet, die mit sehr geringen Eis- und Organikgehalten sowie einer fehlenden organischen Auflage klassifiziert wurde.

Dieser Modellierungsansatz mit Fernerkundungsdaten erweist sich als ein praktisches Werkzeug, um Permafrosttemperaturen im Lenadelta und ihre Änderung über die Zeit mit einer Auflösung von 1 km^2 zu beobachten. Zudem stellt er einen ersten Schritt für weitere operationelle Permafrostuntersuchungen mit Fernerkundungsdaten dar.

Contents

List of Figures

List of Tables

1   Introduction

1.1   Permafrost in the Arctic - an important variable in the global climate

Permafrost is defined as soil, rock or sediment that remains at or below freezing temperature for at least two consecutive years (Harris et al. 1988, van Everdingen 2005). Following this definition, up to 24 % of land area at the Northern Hemisphere contain permafrost (Zhang et al. 2000, see Fig. 1). To further characterize permafrost ground, it is divided into continuously frozen ground and the 'active layer' on top, which is subject to annual freezing and thawing. Additionally, in permafrost regions so-called 'taliks' can occur which are permanently unfrozen layers or bodies in the permafrost ground

Fig. 1: Circum-arctic map of permafrost distribution in the northern hemisphere, indicating the four major regions of permafrost distribution. Brown et al. 1997. The focus region of this thesis, the Lena River Delta, is marked in red.

which usually occur below lakes or rivers or are related to anomalies in the hydrological, thermal, hydrogeological or hydrogeochemical conditions (van Everdingen 2005).

The main driver of the permafrost conditions in the ground is the temperature at the surface. Surface temperatures are influenced by surface and topographic characteristics, like vegetation, snow cover, relief and aspect. Permafrost conditions are also strongly driven by subsurface characteristics, like ground substrate and its moisture and organic contents (French 2007). Therefore, areas with and without permafrost can coexist next to each other on a small local scale. Four major zones are distinguished in the northern permafrost regions (Fig.1): (1) the zone of continuous permafrost with 90 to 100% of the land area underlain by permafrost, (2) the zone of discontinuous permafrost with 50 to 90% permafrost, (3) the zone of sporadic permafrost with 10 to 50 % of permanently frozen ground and (4) the isolated permafrost zone where permafrost occurs in single patches (<10% of the area) in an otherwise unfrozen ground environment. The focus region of this thesis, the Lena River Delta (LRD), is located in the continuous zone of permafrost in Northeast Siberia which represents one of the coldest permafrost regions of the world.

Permafrost ground in the Siberian tundra lowlands, including the LRD, is characterized by very high ice (70 % and more) and organic contents (Romanovsky et al. 2010). Permafrost soils in the tundra lowlands are known to have relatively greater contents in organic carbon because decomposition of organic matter is inhibited by cold temperatures, water saturation and short growing season. About half of the world's below-ground organic carbon stock is stored in permafrost affected soils, where the carbon is protected against microbial decomposition by the cold temperatures (Tarnocai et al. 2009, Schuur et al. 2008).

The recent IPCC report (AR5 2013) suggests present and future warming of the global climate, and increasing mean annual air temperatures have been measured in many regions of the world. Especially in high latitudes, a pronounced warming trend is already observed (Serreze et al., 2000, ACIA 2005, IPCC AR5 2013) and studies suggest an increase of about 4 °C of the yearly mean air temperature since 1954 (ACIA 2004). The observed atmospheric warming also causes the ground to warm successively. When ground temperatures increase as a consequence of warming air temperatures, the active layer deepens and previously frozen organic material becomes exposed to decomposition. As a consequence, greenhouse gases, in particular CO_2 and CH_4, can be released into the atmosphere and may cause a positive feedback for climate warming (ACIA 2005). Historically, tundra ecosystems have been a sink of CO_2 and CH_4 but with the changing climate and warming in the arctic regions, they may change from a sink to a source (Zimov et al. 1997).

The Siberian tundra lowlands with its high ground ice contents are vulnerable permafrost features if it comes to increase in temperatures. Romanovsky et al. (2010) indicated that this landscape type is a key permafrost region that will be strongly affected by climate change.

1.2 Monitoring of permafrost

So far, monitoring of the ground thermal state is restricted to point observations in boreholes and indirect surface observations, e.g. thermokarst occurrence. In-situ monitoring projects, such as the Global Terrestrial Network for Permafrost (GTN-P) (Romanovsky et al. 2010), are one way to observe ground temperatures and active layer thicknesses at the point-scale. The GTN-P is comprised of two components: (1) the Circumpolar Active Layer Monitoring (CALM) for which continuous active layer measurements are undertaken and (2) the Thermal State of Permafrost (TSP) in which ground temperatures are measured in over 500 boreholes with depths ranging from a few meters to more than 100 m. In this thesis, the data of one TSP and one CALM site are used for validation of modeled ground temperatures.

Implementing an even denser network of borehole monitoring sites is labor-intensive and, for environmental reasons, not always desirable. A possibility to infer ground temperatures on large spatial scales is the use of grid-based models that employ climate data as forcing and stratigraphic and vegetation data as input. Spatial permafrost modeling was recently demonstrated by Zhang et al. (2014) for a tundra region in Canada, by Jafarov et al. (2012) for Alaska with the use of climate model data, by Fiddes et al. (2013) for mountainous regions and by Westermann et al. (2013) for Southern Norway with a gridded air temperature product. Such spatially distributed models can assess regional variability due to differences in snow cover and vegetational and soil stratigraphic properties of the ground.

So far, remotely sensed data sets have been of limited value for permafrost monitoring. As permafrost is a subsurface temperature phenomenon, it is not possible to observe it directly from satellite-borne sensors. However, some remotely sensed data sets can be used as input for the above-mentioned permafrost models. For the first time, Langer et al. (2013) demonstrated a permafrost temperature modeling scheme forced by remote sensing data for a point in the Lena River Delta.

For this thesis a similar model scheme is used to map the permafrost temperatures of the entire LRD, based on satellite-derived information on surface temperature and snow. The characteristics of the chosen modeling approach for this work are presented in Chapter 2.

1.3   Outline

The goals of this thesis are

- to establish stratigraphic information for the soil domain of the permafrost model for the entire Lena River Delta. This task is done by evaluating studies performed in that region and deducting a stratigraphy suitable for the use in the model.
- validation of the model forcing data sets (with a particular focus on land surface temperature).
- to perform model runs, calculating permafrost temperatures for the Lena River Delta for the last ten years.
- to validate the modeled ground temperatures and thaw depths with the available in-situ data.

2 Scientific Background

The second chapter focusses on the two main topics of the thesis: first, it provides an overview of the permafrost landscape in tundra lowlands, and the special characteristics of the thermal regime of permafrost soils. The second part gives an introduction into permafrost modeling and its challenges.

2.1 Permafrost in Northeast Siberia

The ground thermal regime in the study area is characterized by continuous lowland permafrost (see map Fig.1). It developed over at least the last hundreds of thousands of years undergoing repeated changes of climate and environmental conditions and as well transgressions and regressions of the sea (Romanovskii and Hubberten 2001). During the last glacial maximum, Northeast Siberia was not covered by glaciers (Fig. 2), but characterized by an extremely cold periglacial landscape which allowed deep permafrost formation (Schirrmeister et al. 2011). Moreover, the global sea level is estimated about 120 m lower than today, leading to a shoreline several hundreds of kilometers north of the present coast coastline. In the cold and dry
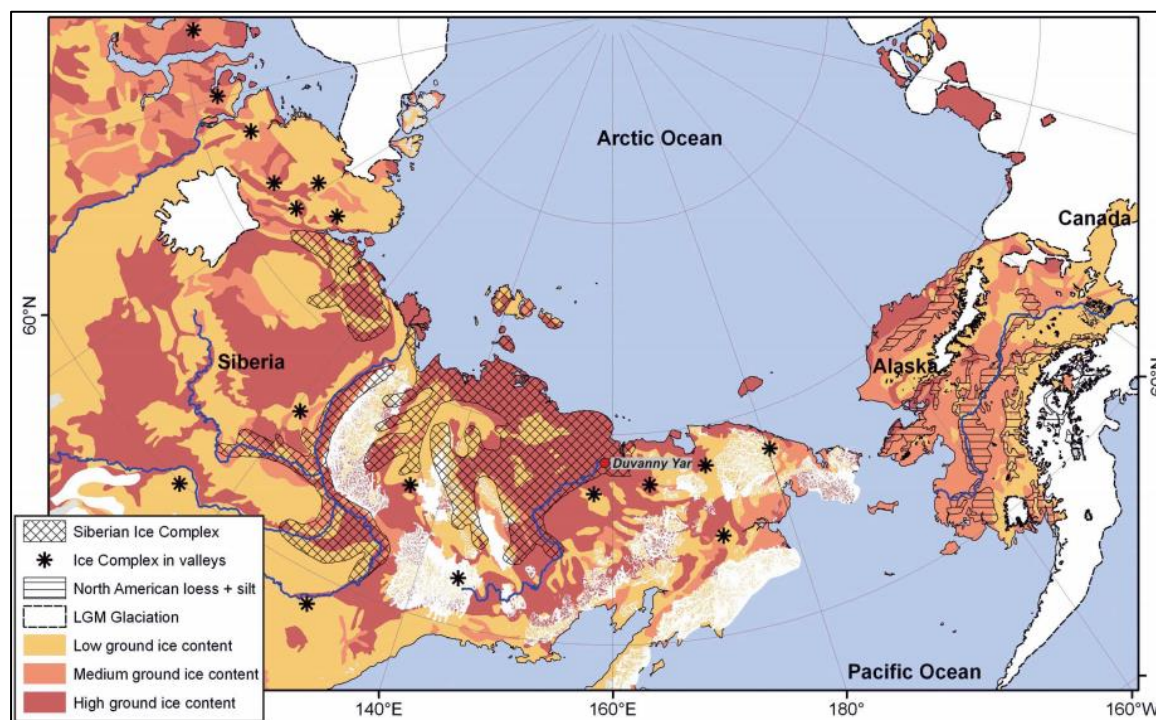
Fig. 2: Extent of Siberian Ice Complex and North American loess deposits in Siberia, Beringia and Alaska, as well as last glacial maximum (LGM) glaciation (Strauss et al. 2012). Siberian Ice Complex is a synonym for Yedoma.

climate permafrost aggradation occurred on the flat accumulation plain of the former Lena river, that formed north of the Chekanovsky Ridge (see Fig. 9 in Chapter 3.2). Today, the thickness of continuous permafrost in the northeast Siberian tundra lowlands is estimated to be 500 to 700 meters (Grigoriev 1960).

Permafrost occurs in several forms in this area, from permafrost in rocks and debris over frozen sandy sediments with low ice and organic content to silty sediments with ice wedges and medium to high organic contents, which creates polygonal patterned ground (Fig. 3). A special geomorphologic form of permafrost is the so called 'Ice Complex' or 'Yedoma' that can be found in lowland permafrost all over Siberia and Alaska (Fig. 2). It typically consists of silt-, organic- and ice-rich deposits of both fluvial and aeolian origin formed in Late Pleistocene. It features thick layers of peat, also in great depth of the profiles, presenting old tundra horizons that have been frozen, as well as syngenetic ice wedges (ice wedges that grow together with the sediment layer) and segregation ice (Grosse et al. 2013). Segregation ice is mainly ice lenses or layers that form in permafrost soils that draw in water while the soil freezes. The ice of the old massive ice wedges of the Yedoma can make out up to 80 % of the soil volume (Schirrmeister et al. 2011).
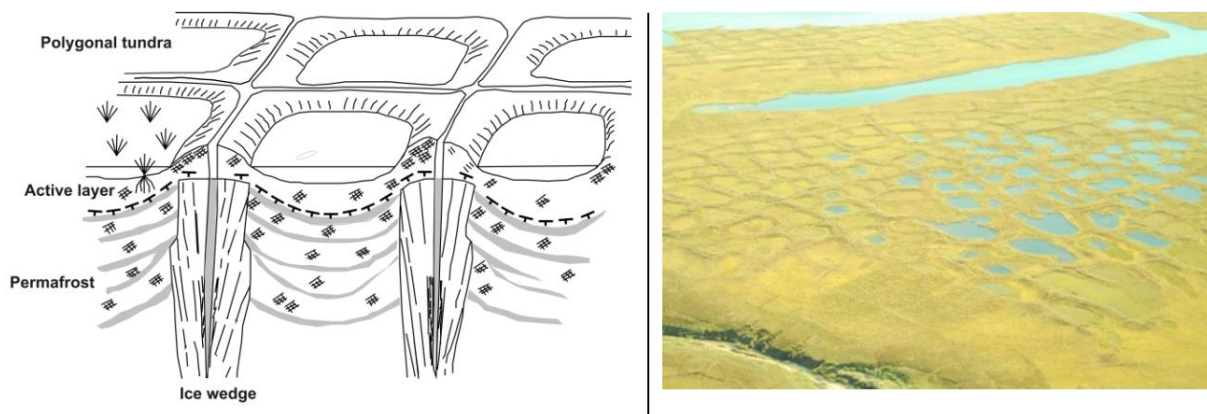
Fig. 3: Left: Scheme of polygonal tundra formed through ice-wedge networks with low-centered polygons, based on Romanovskii (1977), modified by Strauss (2010). Right: aerial photo of polygonal tundra in the Lena River Delta, photo by S. Stettner, AWI 2013.

Furthermore, ice wedges formed during Holocene can be found, but they are younger and thus smaller than those formed during a colder and dryer climate in Late Pleistocene. Today, in a warming climate, permafrost thaw becomes more likely. The thermal regime of the soil is slowly responding to warmer air temperatures (Schuur et al 2009), which leads to formation of many permafrost degradation forms, like thermokarst lakes and alass depressions, thermoerosional valleys (Morgenstern et al. 2012), and thermoerosion of shorelines (Günther et al. 2013). Thermal erosion is generally defined as 'The erosion

of ice-bearing permafrost by the combined thermal and mechanical action of moving water' (van Everdingen 2005). Alasses are depressions in ice-rich permafrost deposits formed through thawing of ground ice. Today they are seen as one stage in a progressive landscape development of a thermokarst relief. Alas development is often connected to formation of thermokarst lakes (French 2007, Washburn 1979).

Fig. 4 displays an example of coastal erosion on Kurungnakh Island, an island of the Lena River Delta. It is one of the islands that are part of the Ice Complex and massive exposed ice wedges can be seen in this outcrop.

Fig. 4: Exposed Ice Complex and part of the underlying sediment facies at Eastern shore of Kurungnakh Island in the Lena River Delta. Photo by S. Stettner, AWI, 2013.

2.2 Thermal regime of permafrost affected soils and ground

To describe the soil thermal regime in a standardized way, several temperature definitions at defined positions in the air-ground profile are used (Fig. 5).
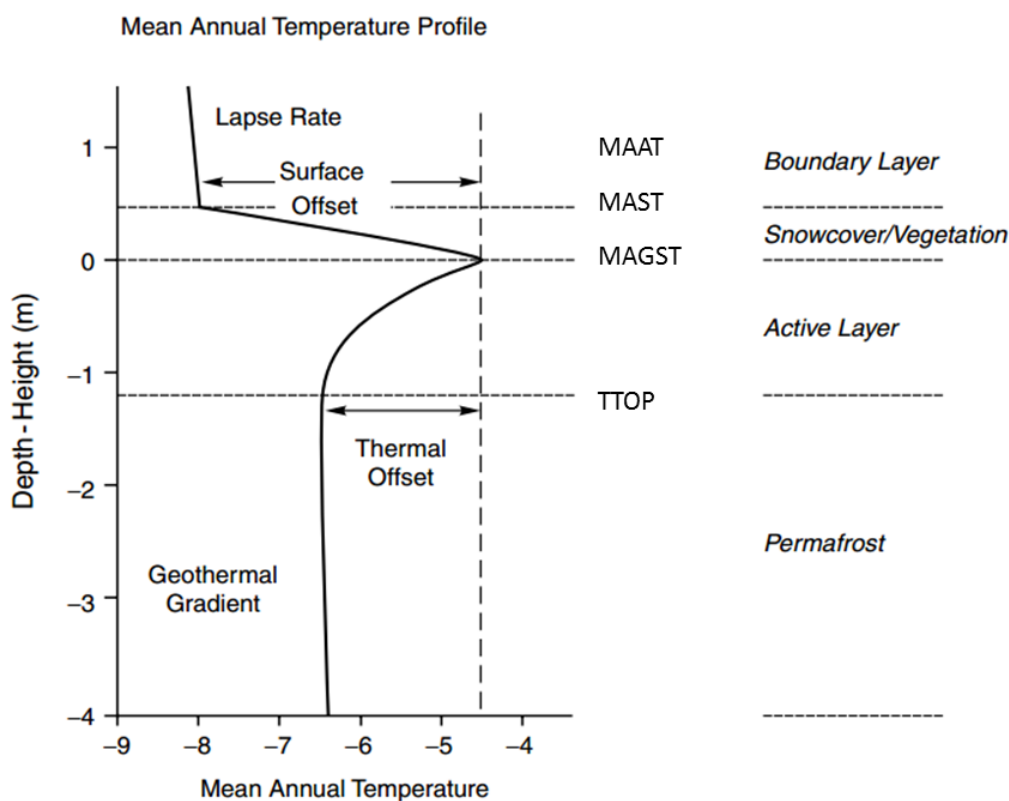
Fig. 5: Scheme of the mean annual ground thermal regime including thermal surface influences. Modified after Smith and Riseborough (2002).

In this graph permafrost with a mean temperature of about -6.5 °C is represented. Above the continuously frozen permafrost table, measured mean annual ground temperatures (MAGT often used as synonym with TTOP) usually rise until the grounds surface. The difference between the temperature on top of permafrost (TTOP) and the mean annual ground surface temperature (MAGST) is called the thermal offset which is caused by the composition of soil and ground material and its different thermal conductivities in frozen and thawed state. The temperature indicator for permafrost TTOP is also used for some simple permafrost models (see below).

If vegetation and/or snow are covering the ground, another inversion in the mean annual temperature regime is detected. The difference between the MAGST and the mean annual

14

surface temperature (MAST) or the mean annual air temperature (MAAT) is called the surface offset and is caused by the insulating effects of vegetation and snow and the effects of a near-surface boundary layer.

While snow cover was identified to play a key role in insulating the ground from cold winter temperatures (Zhang 2005, Farbrot et al. 2013, Langer et al. 2013, Goodrich 1982), vegetation cover is also important for the ground thermal regime. It is also shown (e.g. by Ulrich et al. 2008 and Schneider et al. 2009) that different permafrost forms and stadiums of permafrost degradation bear different kinds vegetation cover and plant communities in the Lena River Delta and in general in permafrost regions (Walker et al. 1977).

For this reason, considerable differences can arise between MAAT and MAGST. Still, MAAT is often used for derivation of permafrost conditions from surface variables. In studies for Norway and Iceland, a MAAT of -3 to -4 °C was shown to be a good estimate to represent the regional lower boundary of permafrost occurrence in mountain areas (Etzelmüller et al. 2003, 2007).

The thermal influence coming from beyond the permafrost table is the geothermal gradient, caused by the heat flow from the interior of the earth, interfering with the influence of heat conduction from the Earth's surface at the lower boundary of permafrost. This gradient is taken into account in the model used in this thesis.

Diagrams showing the characteristics and maximum differences in the annual temperature regime of the ground are used to characterize permafrost regions and are called trumpet-diagrams or trumpet-curves. The trumpet curve shown in Fig. 6 characterizes the thermal regime for Samoylov Island in the center of the LRD. Near the surface, the high temperature range is shown with winter mean values down to -35 °C and up to 18 °C in summer, indicating the continental climate of the site. At the mean-line, the MAGT for every depth is given and at the point where the max-line crosses the 0°C-temperature line, the thaw depth of the site can be inferred. It also maps the depth at which permafrost temperatures are not influenced by seasonal temperature cycles anymore. In the case of Samoylov, this point is reached at about 15 m depth. Due to scale, the geothermal influence is not visible in this graph, but in deeper boreholes it becomes manifest as increasing temperatures with depth. Also, in deep boreholes former climate changes or changes of the thermal regime of the upper ground layers can be detected as a 'bump' or wave in the line of deeper permafrost temperatures. Thus deep ground temperatures can function like an archive for long-term temperature changes (Mottaghy et al. 2013).
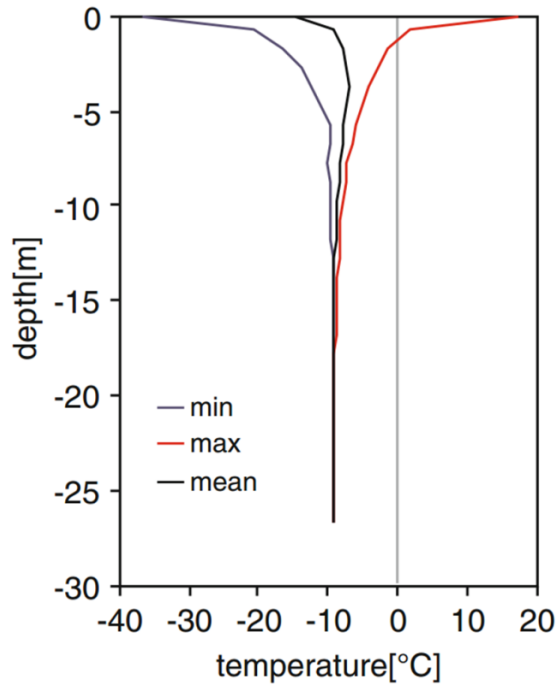
Fig. 6: Trumpet curve for 2006 to 2011 for a 26-m deep borehole on Samoylov Island, an island in the center of the LRD, with mean, maximum and minimum temperatures (Boike et al. 2013).

2.3 Permafrost modeling – approaches and comparison of models

There are various modeling approaches that differ in input and output variables, accuracy, uncertainty and complexity. These factors have to be taken into account and well regarded when choosing the suitable model for the research question.

Riseborough et al. (2008) evaluated the recent advances in this field of permafrost research. They compared permafrost modeling approaches regarding thermal, spatial and temporal criteria.

Empirical models are statistical models that connect permafrost occurrence or its physical variables to specific environmental factors, such as mean air temperature or altitude, using empirically derived relationships. They are mainly used for mountain areas, e.g. by Hoelzle et al. (2001) to provide mean permafrost temperatures or probability maps. Empirical models have also successfully been applied to lowland permafrost in Alaska (Shiklomanov and Nelson 2002).

Equilibrium models define permafrost conditions in equilibrium with a given annual climate regime. They can hence not represent transient responses of the ground thermal

16

regime to the evolution of the climate. A widely used example is the TTOP-model (Smith and Riseborough 1996) which relates MAGT to MAAT (see Chapter 2.2) using transfer functions.

In contrast to equilibrium models *transient permafrost models* can capture the temperature evolution over time, starting from some initial state. They generally simulate a vertical ground temperature profile by numerically solving the heat transfer equation (see Chapter 4.1. for more details). They are sufficiently flexible to deliver realistic results for a wide range of permafrost and climate conditions (Riseborough et al. 2008). In this work, the transient model CryoGrid 2 (Westermann et al. 2013) was used to spatially model the ground thermal regime of the Lena River Delta.

Common to all models is the need of driving data sets of meteorological or surface variables such as air temperature. These data sets can vary in scale depending on the application and the source from which they were derived. For point-scale application input data from in-situ measurements are often used (e.g. Roth and Boike 2001). To obtain maps of permafrost variables spatially distributed data sets are required. Hereby, the scale of the input data sets also defines the scale of the model output. They range from 1km^2 or less (e.g. for gridded air temperature data sets, derived by interpolation between climate stations, Westermann et al. 2013) to the output of General Circulation Models (GCM) which is only available at coarse scale of e.g. 1.4 ° x 1.4 ° of latitude and longitude, as in Lawrence and Slater (2005).

Also remote sensing data sets have already been used by Langer et al. (2013) on 1km^2 – scale as input for a transient model and by Hachem et al. (2008) who used MODIS LST as input for an equilibrium model to derive the zonation of continuous, discontinuous and sporadic permafrost over Northern Quebec, Canada.

3 Study region

3.1 Overview
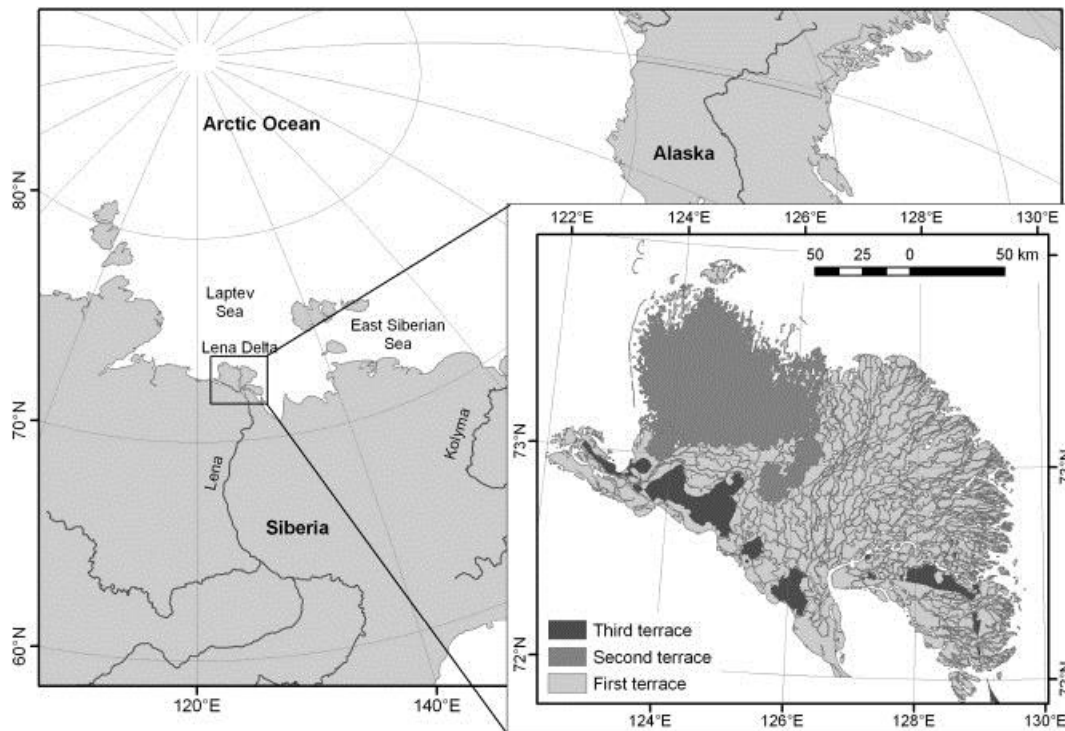
Fig. 7: Location of the Lena River Delta in Northeast Siberia and outline of river terraces (small frame). From Schneider et al. 2009, based on Schwamborn et al. 2002.

The Lena River Delta is located at the coast of the Laptev Sea in Northern Siberia (72.0–73.8° N, 122.0–129.5° E, Fig. 7). With an area of 32.000km^2, it is the largest arctic river delta in the world, highly dissected by rivers and streams and composed of more than 1,500 islands (Are and Reimnitz 2000, Walker 1998). Its four main river channels, Olenyoskaya, Tumatskaya, Trofimovskaya and Bykovskaya, are draining to the west, north, east and southeast, respectively (Fig. 10).

The delta is situated about 100 to 150 km north of the arctic tree line in the arctic tundra lowlands. The tundra vegetation consists of shrubs and mini-shrubs, as well as several moss, grass and sedge types (Schneider et al. 2009). The climate is characterized as polar tundra climate, according to the Köppen-Geiger classification. Data from the meteorological station on Samoylov Island showed a MAAT of -12.5 °C, while the mean

air temperature in January is around -30 °C and around 10 °C in July, indicating a large temperature range of about 40°C typical for arctic continental regions (Boike et al. 2013). A pronounced variability of the summer climate, especially of precipitation, is observed which is caused by the varying influence of either moist and cold air masses from the Ocean or dry and warm air masses from Central Siberia (Boike et al. 2013). Mean annual precipitation of about 200 mm with variations on the order of 150 mm, are documented for Samoylov Island (Boike et al. 2013). Moreover, only about 30% of the annual precipitation occurs in the form of snow, leading to a rather shallow snow depth. The snow cover season usually begins between the end of September and October and ends between May and beginning of June. Snow melt is observed to occur very fast within one week, as documented for Samoylov Island in the center of the Delta (Langer et al. 2013) and for the whole delta for the year 2012 (Peter 2014).

Polar day starts on May 7th and ends on August 7th, whereas polar night begins on November 15th and ends on January 28th in the Lena River Delta.

Situated in the continuous permafrost zone, the permafrost table is estimated to reach depths of 500 to 600 m in this region (Grigoriev et al. 1996). With ground temperatures as low as -12°C, the study area is among the world's coldest permafrost regions (Kotlyakov & Khromova 2002). Annual maximum thaw depths, i.e. the deepest extent of the active layer in summer, range from about 0.2 to 1.0 meters in the Lena River Delta region (Zubrzycki 2013). Geomorphologically, the delta can be divided into three river terraces that differ in genesis, composition of soil constituents and vegetation cover (see below).

The study area was chosen due to the availability of in-situ measurements which is found seldomly in the remote regions of northern Siberia. Some of these measurements started as early as 1993, when studies started to focus on the Lena River Delta. Since then, the LRD has been the target of a number of expeditions, enabling the maintenance of measurement stations and providing the basis for ongoing research. This provides the chance to validate modeled results with measured data. Secondly, a number of vegetational, geomorphological and geological studies have been performed in the delta and nearby regions which facilitate estimating the stratigraphic classification required for the soil domain of the model. There have been qualitative studies on permafrost and the distribution of permafrost in the Delta area, focusing on soil constituents and soil organic carbon of the upper tundra soil, degradation of permafrost and thermokarst forms, as well as sedimentological history and paleo-studies on permafrost deposits and delta evolution. An overview for the research observatory on Samoylov Island in the southern center of the delta is found in Boike et al. (2013).

3.2 Geology, Geomorphology and Vegetation

The modern delta is based on alluvial deposits of the Lena River and quaternary sediments that, in some places, extend down to 100 m depth (C. Siegert, pers.comm. based on Gusev 1961). Maps based on geophysical exploration suggest 1000 to 4000 m deep sediments from Cretaceous to Cenozoic deposits that underlie the delta (Schwamborn et al. 2000, Grigoriev et al 1996).

First terrace

The Lena Delta is geomorphologically composed of three main river terraces that differ in genesis and stratigraphy. The first river terrace of the Lena River is characterized as the active and youngest part of the delta and formed during the late Holocene (Schirrmeister et al. 2003, Schwamborn et al. 2002). It covers wide parts of the eastern and central delta. It can be subdivided into a floodplain level, 0 to 4 m.a.s.l. (above sea level), and the late Holocene river terrace, up to 12 m.a.s.l. (Akhmadeeva et al. 1999, Langer et al. 2013). Here, polygonal tundra dominates, with ice wedges reaching a depth of up to 9 meters (Schwamborn et al. 2002) or 10 to 15 meters (Langer et al. 2013, Grigoriev et al. 1996) depending on the location in the delta. The soil and sediment material of the first terrace consists of silty sands and great amounts of organic matter in alluvial peat layers that reach thicknesses up to 5 to 6 m (Schwamborn et al. 2002b/supplement). A medium thick organic layer of 10 to 15 cm features the upper soil horizon. Volumetric ice contents of the peat soils are reported to reach values of 60 to 80 vol %, mineral contents of investigated sites range from 20 to 40 vol % and the organic contents 5 to 10 vol % (Kutzbach et al. 2004, Zubrzycki et al. 2012). The cryo-organic soil complex is underlain by silty to sandy river deposits (Boike et al. 2013).

Zubrzycki et al. (2013) analyzed the volumetric ice content for soils on the active floodplain and on the Holocene river terrace with measurements in six different depths of a 100 cm deep profile. The mean for all values of the profile is 51.16 vol % for the first 100 cm. Minke and Kirschke (2007) estimated the mean volumetric water content for the soil of 5 sites of the floodplain of Samoylov Island during Expedition to the Lena Delta in 2006. They calculated a mean water content of 40 vol %. Organic layers were not documented for the mineral soil of the floodplain.

The tundra surface covering the first terrace is characterized by grass, moss and occasional dwarf shrubs (see Fig. 8, Schneider et al. 2009). Generally, Langer et al. (2013) describe the vegetation of the higher elevated alluvial first river terrace as typical

polygonal tundra vegetated by mosses and sedges with a medium thick tundra horizon. Kutzbach et al. (2004) described the plant community of one polygon on Samoylov Island in the central Lena Delta. They documented 5 cm high mosses and lichen and up to 30 cm high vascular plants for the center and a 5 cm high dry moss and lichen stratum and 20 cm high vascular plant stratum for the polygon rim. The total coverage of vascular plants was relatively low with about 30 % and the moss- and lichen stratum was high with 95 % coverage of the area of the investigated
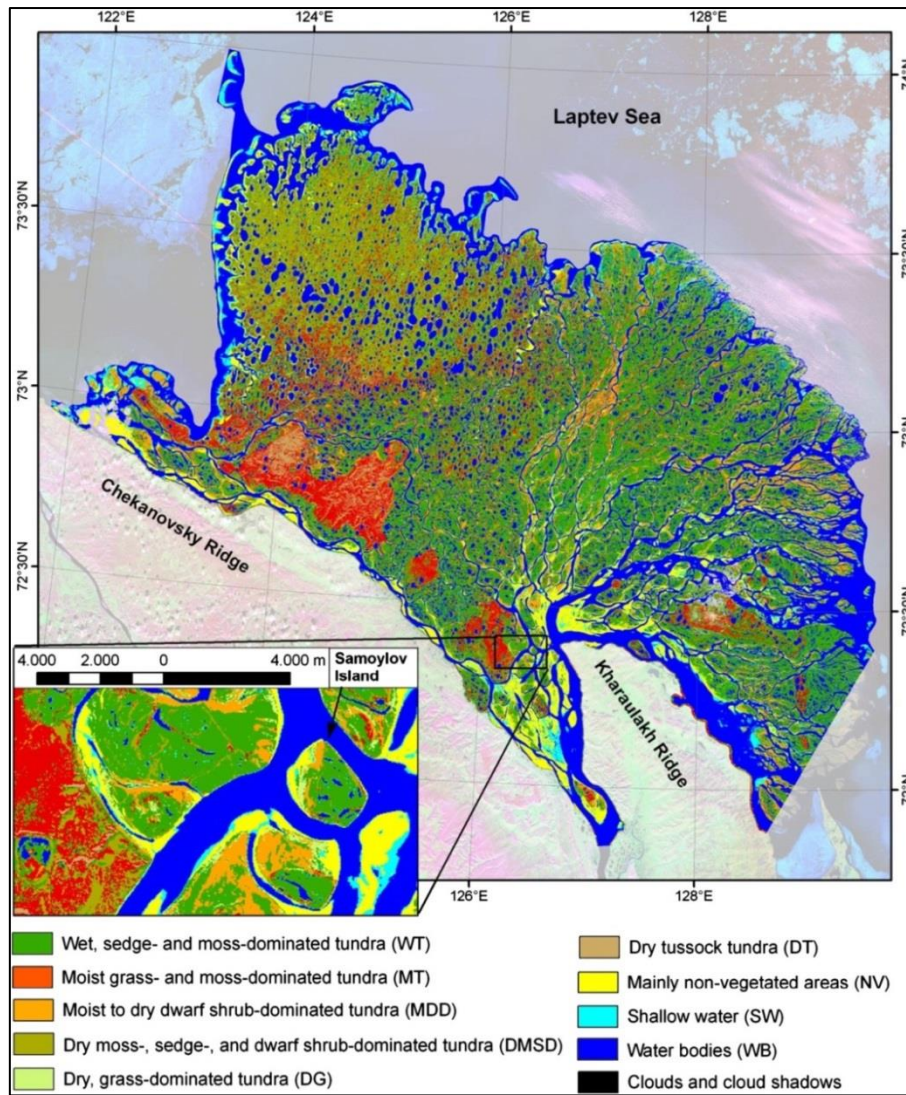
Fig. 8: Land cover classification based on Landsat satellite images, 30 m resolution, by Schneider et al. 2009.

polygon. Boike et al. (2013) have classified the wet tundra as a '*Drepanocladus revolvens-Meesia triquetra-Carex chordorrhiza* community' and the dry tundra as a '*Hylocomium splendens-Dryas punctata*-lichen community' on Samoylov Island.

For the floodplain, the classification of Schneider et al. (2009) mostly assigns the classes 'Dry, grass-dominated tundra', 'Moist to dry dwarf shrub dominated tundra' and 'Mainly non-vegetated areas' to this type of geomorphologic unit. During the expedition LENA 2006, Minke & Kirschke (2006) characterized the vegetation of the floodplain as part of Samoylov Island as "mesic tundra vegetation, dominated by herbs (*Hedysarum arcticum, Festuca rubra, Deschampsia borealis*) and shrubs (*Salix reptans, Salix glauca*). Mosses and lichens are absent.

Second Terrace

The second river terrace (10 to 30 m.a.s.l.) is mostly found in the western and northwestern part of the delta. It was generated during marine isotope stage 2 and transition to 1, when the sea level was lower than today and the deposits accumulated in a continental setting, and is now an inactive part of the delta. The biggest island created by this river terrace is called Arga-Island and for this reason the second terrace is often referred to as Arga-complex. The ages of a core taken from Arga Island, analysed through IR-OSL analysis, vary from 12 to 13.4 ka BP (Schwamborn et al. 2002) and deep deposits of this terrace reach ages of >50 ka BP (Schirrmeister et al. 2011). The second terrace is mainly characterized by sandy mineral material, low ice (30 vol %) and organic content and the lack of an organic upper layer (Schirrmeister pers.comm., Rachold and Grigoriev 1999). There exists a theory that varying river runoff and possibly tectonic uplift led to different sedimentary composition of the terrace (Schirrmeister et al. 2010, Schwamborn et al. 2002). Cryogenically, the deposits of the second terrace are characterized by nets of narrow-standing (dm-scale) ice veins and segregational ice (Schwamborn et al. 2002, Rachold & Grigoriev 1999). The polygonal microrelief is less expressed and deep, oriented thermokarst lakes are typical (Rachold & Grigoriev 1999, Morgenstern et al. 2008). Sparse vegetation cover and up to 50% bare areas are also typical for the 2nd terrace (Ulrich et al. 2009, Schneider et al. 2009). If vegetation is present it is expressed in a micro-hillocky surface with *artemisia sp., papaver pulvinatum, salix nummularia* and others. No organic layer on the mineral soil is found (Rachold and Grigoriev 1999).

Third terrace

The third river terrace is composed of patchy residual parts (islands) in the southwestern, southern and southeast part of the delta, rising up to 55 m above the summer river level (Zubrzycki et al. 2012, Grigoriev 1993). Referring to 14C and IR-OSL age determinations, the main delta channel accumulated sediment there during isotope stages 5 to 3 (Schwamborn et al. 2002, Kuzmina et al. 2003). Between 43 and 14 ka BP, the

growth of the so called 'Ice Complex' or 'Yedoma' reached its maximum, creating syngenetic ice wegdes and massive ground ice within peaty sandy silts, the peat layers extending to a depth of up to 7-11 meters below the surface. The lower boundary of the Ice complex is documented to be found between 15 to 20 m depth (Schirrmeister et al. 2011). For the third terrace ice wedge depths of up to 20 to 25 m are described (Schirrmeister et al. 2003, Grigoriev 1993, Schwamborn et al. 2002). The vegetation consists of thick 10 to 20 cm hummocky grass, sedge and moss cover, in some places shrubs. The upper horizon of the soil has a thick organic layer (Schneider et al. 2009).

In the whole delta area, periglacial landforms, like permafrost thaw lakes, thermokarst forms, polygonal tundra and pingos, are present (Morgenstern et al. 2008, Ulrich et al. 2009). Due to different composition of the terrace units, permafrost degradation and thermokarst occurs in different stages and forms, depending on the river terrace. This means there are for example relatively more thaw lakes on the 1st than on the 3rd terrace or different development of thermo-erosional valleys.

4   Methods

This chapter introduces the tools and methods that were used to obtain modeled ground temperatures for the region of the Lena River delta. First the numerical model is described, then the required driving data and the methods to acquire them are explained. The second focus is set on the model set-up. Finally, in-situ measurements employed for validation are described.

4.1   Model description

For transient modeling ground temperatures, the 1D soil heat transfer model CryoGrid 2 (Westermann et al. 2013) was used. It is capable of representing the annual build-up and disappearance of the snow cover, as well as the freezing and thawing of the active layer. A detailed mathematical description and numerical solution methods can be found in Westermann et al. (2013), and here only an overview of the governing equations of the soil heat transfer is given.

The numerical solution of the model is based on equations of the conductive heat transfer that includes a term for the phase change of soil water (Jury and Horton 2004, Yershov 1998).

$$c_{eff}\,(z,T)\,\frac{\partial T}{\partial t}\, -\, \frac{\partial}{\partial z}\left(k(z,T)\frac{\partial T}{\partial z}\right) = 0$$

Hereby, t denotes time [s], z depth [m], T (z,t) ground temperature [°C] and k (z,T) the thermal conductivity [Wm^{-1} °C^{-1}]. The temperature-dependent effective volumetric heat capacity c_{eff} (z,T) [J m^{-3} °C^{-1}] accounts for the latent heat of freezing and melting of water as follows,

$$c_{eff}\, = c\,(z,T) + L\,\frac{\partial \theta_w}{\partial T}\ ,$$

where θ_w [-] is the volumetric water content and L=334 MJ m^{-3} is the specific volumetric heat of fusion of water. The term c (z,T) is calculated from the volumetric heat capacities c_α [J m^{-3}°C^{-1}] and the volumetric fractions θ_α of the ground constituents α = water, ice, mineral, organic, air as

$$c\,(z,T) = \sum_{\alpha} \theta_{\alpha}\,(z,T) c_{\alpha}$$

The latter were defined in the stratigraphy of the model ground domain (see Chapter 5.1). They are also used to calculate the temperature and depth dependent thermal conductivity

$$k(z,T) = \left(\sum_{\alpha} \theta_{\alpha}(z,T)\,\sqrt{k_{\alpha}} \right)^2$$

according to Cosenza et al. (2003). k_{α} denotes the thermal conductivities of the individual ground constituents.

CryoGrid 2 needs forcing or driving data sets which are time series of surface temperatures and snow depth or snow water equivalent. In addition, a number of parameters must be specified, in particular the properties of the ground and the snow. In this thesis, CryoGrid 2 was used with the forcing data proposed by Langer et al. (2013), i.e. using remotely sensed data of the land surface temperature LST and snow water equivalent SWE as forcing (Fig. 9). These forcing data and the model runs were generated in an established and standardized way on a supercomputing cluster at the University of Oslo, Norway. For the crucial input data set of the ground properties, such standardized methods are not available (see Westermann et al. 2013). Therefore, it was manually compiled for the study area as a key part of this thesis (Chapter 5.1).
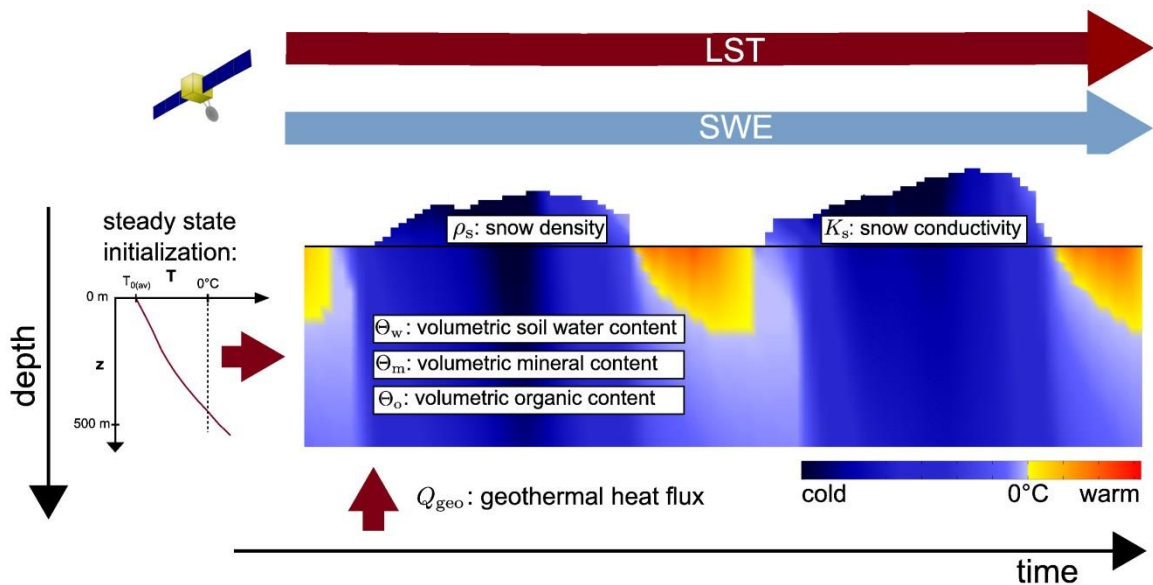
Fig. 9: Model scheme featuring forcing data and ground properties (Langer et al. 2013).

4.2   Forcing Data

As driving data, time series of Land Surface Temperatures (MOD11A1/MYD11A1 daily, level 3, collection 5) and GlobSnow Snow Water Equivalent, as well as Snow extent (GlobSnow SWE daily, MOD/MYD10A1, level 3, version 5) were used. All products are available in the same time window over about 10 years and thus suitable for a long term forcing data series. The employed time series starts at 15th July 2002 and ends 1st September 2011, featuring weekly averages. All forcing data series were generated in a readily implemented way on the Abel Supercomputing Cluster at the University of Oslo, following the procedures and algorithms described in Langer et al. (2013).

4.2.1 MODIS LST

For the land surface temperature the product MOD11A1 Daily L3 V005 from satellite 'Terra' and the product MYD11A1 Daily L3 V005 from satellite 'Aqua' was employed. Both provide daily information of Land Surface Temperatures and Emissivity. The MODIS LST product comes in a sinusoidal projection with tiles of a resolution of about 1x1km and 1200x1200 (rows x columns) pixels. MOD11A1 data are available since March, 5th 2000 and MYD11A1 since July 8th 2002 until present. For the location of Lena River Delta, the time series of tile 'h21v01' was used. The hdf files contain 12 data layers of which only Daytime Land Surface Temperature and the Nighttime Land Surface Temperature are used. From the available daytime and nighttime values, a time series of weekly averages was compiled by averaging over all available data (Langer et al. 2013).

This satellite product is sensitive to cloud cover and thus it is not able to provide information if the scene is covered with clouds. This can lead to biased values and overrepresentation of cold temperature values in the time series (Westermann et al. 2012), especially in arctic and subarctic regions and during polar night. The warmer land surface temperatures that can occur during cloud cover cannot be measured, while the colder temperatures in clear sky conditions can be measured. To counteract this effect, a second version of the temperature forcing was generated, where the gaps in the MODIS LST time series due to cloudiness were filled by near-surface air temperatures from the ERA-interim analysis (see below). For this procedure, ready-made scripts available at the University of Oslo were used. Therefore, two independent model runs are available (see Chaper 5.2)

4.2.2 ERA-interim

ERA-interim is a climate reanalysis product derived from a numerical weather prediction model in which numerous meteorological observations are assimilated. ERA-interim is

provided by the European Centre for Medium-Range Weather Forecast (ECWMF) with a spatial resolution of 1.5° x 1.5°. ERA-interim delivers a 6-hourly representation of atmospheric products from 1st January 1979 to the present. The atmospheric products are available for 60 vertical (pressure) levels (http://www.ecmwf.int/en/research/climate-reanalysis/era-interim, http://www.ecmwf.int/en/forecasts/datasets/era-interim-dataset-january-1979-present).

The ERA-interim product has been validated to produce reliable air temperatures for the Arctic (Screen & Simmonds 2011). To fill the gaps in the MODIS LST product, the 2 m air temperature was downloaded from http://apps.ecmwf.int/datasets/data /interim_full_daily/. From the merged time series, weekly averages were calculated as forcing data for CryoGrid 2.

4.2.3 Snow

To get a daily time series of snow depth data a snow depth product was compiled from the Snow water equivalent (SWE) product of GlobSnow (25x25km) and the Modis Snow Cover product MOD10A1 and MYD10A1 (500x500m) (Snow Extent). Using the method described in detail in Langer et al. (2013), these driving data for snow depth could be scaled to the same grid size like the surface temperature data.

GlobSnow SWE

The GlobSnow SWE (Daily L3A SW) data are available from 1979 to 2011 in daily temporal and at 25x25km spatial resolution. It comes in a single data field for the whole Northern Hemisphere (though limited to 35° to 83° for physical reasons) in the Equal-area scalable Grid – projection (EASE-Grid), so that the data field has a size of 721x721 (columns x rows) pixels. It is accessible through the GlobSnow website (www.globsnow.info).

The retrieval algorithm of the GlobSnow SWE product has been developed and validated by the Finnish Meteorological Institute for tundra landscapes. The input data for the SWE product base on three different passive microwave sensors from different satellites- SMMR (Nimbus -7 Scanning Multichannel Microwave Radiometer), SSM/I(Special Sensor Microwave/Imager – aboard several DMSP-satellites) and SSMIS.

MODIS Snow Cover

The Snow Cover products MOD10A1 V005 and MYD10A1 V005 are daily satellite products with a resolution of 500 m, coming from either the satellite Terra (MOD) or the satellite Aqua (MYD). As the MODIS LST data, it is available in the hierachical data format (.hdf) in a sinusoidal projection, containing 4 image layers. The 4 layers of the image, that show 1200x1200km of area with a pixel size of 500x500m, are snow cover daily, snow albedo daily, snow spatial quality assessment, fractional snow cover. For the modeling, only the first layer 'snow cover daily' was used. Since this product is sensitive to cloud cover because of the optical sensor, data gaps are present in this time series. Here again, the available daily values were used to construct weekly averages.

The MODIS Snow Extent product helps correcting the coarse-scale GlobSnow SWE product regarding start and the end of snow cover period. The resulting forcing time series of snow depths has a finer resolution and the uncertainty about snow covered or not snow covered conditions can be reduced. For coarse grid cells the generalization of 'snow' or 'no snow' gives rise to a high uncertainty especially in the end and the beginning of the snow cover season, when low snow heights cover only parts of the grid cells.

4.3 Model set up

A spatially distributed representation of the soil domain of the model was constructed based on studies conducted in this region (see Chapter 5.1). The extent of the soil domain is from 0 to 600 m depth, containing 104 vertical grid cells. The smallest grid cells of 2 cm start at the surface, while grid cell size increasing with depth to up to 100 m at the bottom to account for larger temperature gradients in the upper part of the stratigraphy/close to the surface. Additional grid cells each spaced with 2 cm are constructed above the ground surface to define the presence of snow cover (see Westermann et al. 2013 for details).

The model is forced at the upper boundary that is set by the ground or snow surface. The lower boundary is set to be at 600 m, because the permafrost table is supposed to reach down to 500 – 600m in this area (Zhang et al. 1999). Here, a constant geothermal heat flux Q_{geo} of 0.053 Wm^{-2} is applied. This value has been measured in a deep 600 m borehole 140 km east of Samoylov Island (Langer et al. 2013).

The snow cover is assumed uniform and constant in its properties in each grid cell, with the values oriented at field measurements (Langer et al. 2013). Soil moisture is assumed to be constant and only changes due to freezing and thawing.

To start the model runs with realistic ground temperatures at the beginning of the model period a model spin-up was done using an initialization procedure of several steps, as described in detail in Westermann et al. (2013). Since only nine years of forcing data were available the entire time series was used for the spin-up. The short spin-up period used in this work is the reason why modeled ground temperatures below 10 m depth are not discussed, because for the representation of those longer spin-up periods are needed.

4.4   Field measurements for validation

On Samoylov Island an intensive measurement program is conducted each year. This program and the measurement installations (Boike et al. 2013) form the basis for the model validation (Chapter 5.3). The other validation sites in the Lena River Delta and the available data are described in more detail in the Result section.

Ground Temperature

Soil temperature measurements are taken using geoprecision temperature chains or hobo-4-channel sensors that are installed in a borehole or close to the soil surface over a period of time. Subsequently the temperatures recorded by the sensors in each depth can be downloaded when the temperature chain is retrieved or the borehole site is visited during expedition campaigns.

Surface Temperature

On Samoylov Island the surface temperature data has been measured continuously since 2002 by a down facing long wave radiation sensor (CG1, Kipp & Zonen, Netherlands). The outgoing long wave radiation is converted into surface temperature using Stefan-Boltzmann law.

Snow Depth

Snow depth measurements have been made by an ultra-sonic ranging sensor (SR50, Campbell Scientific, USA) for one point at the Samoylov Site from 31.08.2002 until 09.04.2011 with few interruptions. This sensor is located close to the long wave radiation sensor.

Thaw Depth

Thaw depth measurements were performed using manual probing with a thaw depth probe, usually at the end of summer (August), when the active layer thickness is assumed to reach the yearly maximum.

5   Results

As a first step, a soil stratigraphy map of the Lena River Delta was developed to deliver soil characteristics as key input for the model. Secondly, the forcing data of the model, in particular MODIS LST, are evaluated and validated against the available field data. Finally, the model results on the ground thermal regime are presented and validated against in-situ observations.

5.1   Definition of soil stratigraphy for CryoGrid 2

From the description of the delta morphology and lithology from several sources, a stratigraphy with volumetric contents of water/ice, mineral, organic and air was derived (Table 1). Three classes are distinguished, which closely follow the outline of the three river terraces (Chapter 3.2).

The Holocene river terrace and the active floodplain as mentioned by Langer et al. (2013) were merged to create the first stratigraphic class, as for the model the differences are often on a too small spatial scale. For the first class, an upper layer of 15 cm with the volumetric contents of 55% water/ice, 10% mineral, 15% organic and 20% air represents part of the vegetation cover and the a-horizon – mineral soil interface, based on Schneider et al. (2009) and Kutzbach et al. (2004). It is also based on documentation of a medium thick 10 to 15 cm tundra horizon for the first river terrace. In the layer below, from 15 cm to 9 m, organic-rich tundra soil with peaty and silty fluvial sands, silty-sandy peats and polygonal ice-wedges are generalized with 65% water/ice, 30% mineral, 5% organic and 0% air volumetric content, based on Schwamborn et al. (2002), Schirrmeister, Grigoriev (1996) and Zubrzycki et al. (2013).

Table 1: Classification with volumetric contents of the ground constituents for the model stratigraphy.

	depth in [m]	water/ice [vol.frac]	mineral [vol.frac]	organic [vol.frac]	air [vol.frac]	Type
class 1 1st terrace	0-0.15	0.55	0.1	0.15	0.2	grass, moss, mini-shrubs
	0.15-9	0.65	0.3	0.05	0	silty peaty sand
	> 9	0.25	0.7	0.05	0	fine sand
class 2 2nd terrace	0-600	0.3	0.7	0	0	fine sand
class 3 3rd terrace	0-0.20	0.3	0.1	0.1	0.5	grass-moss, shrubs
	0.20-20	0.70	0.25	0.05	0	peaty, silty, partly sand
	> 20	0.3	0.65	0.05	0	fine sand

The following sediment layer, which is defined to reach until the lower boundary of the model domain at 600 m depth, is parameterized by 25% water, 70% mineral, 5% organic and 0% air content (Schwamborn et al. 2002, Langer et al. 2013). According to Langer et al. (2013) and Boike et al. (2013) on the first terrace below 20 m of depth the sediment is assumed to be uniform and consists of fluvial silty sands with an estimated pore volume of 20% wich is completely saturated with water/ice.
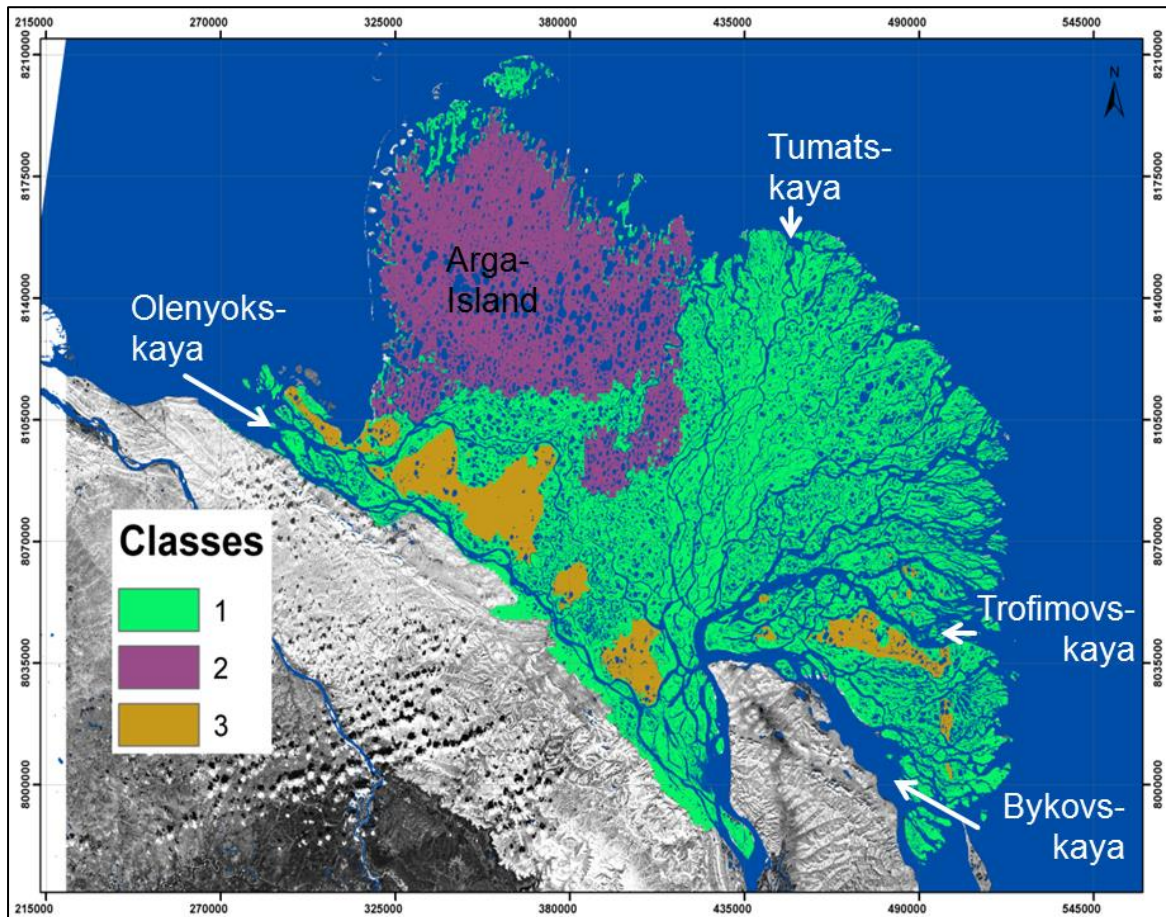
Fig. 10: The stratigraphic classes defined for the model; additionally the main river channels and location of the Arga-Island are indicated. UTM zone 52N. Base map and water masks are according to Chapter 5.1.1.

For the second class, located mainly on Arga Island in the NW part of the Lena Delta, a uniform stratigraphy has been assembled, due to no major vertical changes. From 0 to 600 m depth values of 30% water/ice, 70% of mineral volumetric content have been chosen, based on Schwamborn et al. (2002) and Schirrmeister (pers.comm.) and Rachold and Grigoriev (1999).

The third class largely coincides with the Ice Complex (Chapter 2.1). It is characterized by a slightly thicker vegetation cover and tundra soil than the first class. The near-surface stratigraphy from 0 to 20 cm is 35% water/ice, 10% mineral, 15% organic, 40% air, as described in Schneider et al. (2009) with dry moss- sedge- and dwarf-shrub dominated

tundra and dry grass-dominated tundra. From 20 cm to 20 m depth, thick, organic-rich tundra peat layers with sandy silts and massive polygonal ice wedges are represented with: 70% water/ice, 20 % mineral, 10% organic, 0% air (after Schwamborn et al. 2002), which represents the ice-rich ground conditions typical for the Ice Complex. From there down to the bottom of the permafrost table 30% water/ice, 65% mineral, 5 % organic and 0% air is assigned as this sediment layer is also assumed to be fully saturated (Langer et al. 2013, Schwamborn et al. 2002).

Inquiries have been made to find out the exact volumetric air content in the ice of ice wedges in the Lena River Delta. Dr. Hanno Meyer/Dr. Thomas Opel (AWI) started to measure these values using ice cores from the first river terrace. So far it was estimated that ice wedge ice from the upper 2 m of the soil column contains about 1% of volumetric air content. Still, there is no publication on this and measurements have to be continued, to get accurate values. Therefore, these estimates were not taken into account for the stratigraphy of the model. In addition, a 1% change in the ice content would presumably not affect the modeled temperatures.

The stratigraphic classification map has served as a deliverable in the EU-project PAGE 21 (www.page21.eu) and will be used as input for other permafrost models in the future.

5.1.1 Cartographic implementation

Intensive research about the geologic structure of the Lena River Delta showed that the first river terrace (and floodplain level) can be generalized to stratigraphic class 1. The outlines of the first terrace were digitized based on the map of 'Permafrost Landscapes of Yakutia, Federov et al. (1989)'. In the end, a 1x1 km-gridded map of the Lena River Delta with attributes of either stratigraphic class one, two or three was created. For polygon shape creation, merging, modification of data and gridding, ArcGIS Esri, licensed to Alfred-Wegener-Institute for Polar and Marine Research, was used. Terrace outlines of terrace two and three in vector data type were used and downloaded from the data source database PANGAEA (Publishing Network for Geoscientific & Environmental Data) as they have the same spatial extent like stratigraphic classes two and three.

For further presentation in maps, the MODIS water mask was used to represent ocean and greater rivers and a 30-m resolution water-mask was used to represent ponds, thaw lakes and smaller river arms of the Delta. The base map on which the modeling results are displayed is based on a Landsat Mosaic from 2000 (see Fig. 10).

Meta data information:

GIS-shapes:

- Shape of class 2 and class 3 based on: Morgenstern, A., Röhr, C., Grosse, G., Grigoriev, M.N. (2011): The Lena River Delta - inventory of lakes and geomorphological terraces. *Alfred Wegener Institute for Polar and Marine Research - Research Unit Potsdam*, doi:10.1594/PANGAEA.758728.

- shape for class one was digitized based on: Federov A.N., Botulu T.A., Varlamov S.P. (1989) Permafrost Landscapes of Yakutia. 1: 2 500 000. Yakutian ASSR, Novosibirsk, GUGK, 170p.
  and: Landsat-7 ETM+ mosaic (see base map and water mask).

Base map and water mask:

- MODIS water mask: Carroll, M., Townshend, J., DiMiceli, C., Noojipady, P., Sohlberg, R. 2009. A New Global Raster Water Mask at 250 Meter Resolution. International Journal of Digital Earth. (volume 2 number 4) (tile: MOD44W_Water_2000_XW5152.tif)
- water body mask extracted from the Lena River Delta Land Cover Classification from Schneider et al. (2009) with a resolution of 30m
- Landsat-7 ETM+ mosaic, displayed in bands 1-1-1, based on: MDA Federal (2004), Landsat GeoCover ETM+ 2000 Edition Mosaics Tile N-52-70.ETM-EarthSat-MrSID, 1.0, USGS, Sioux Falls, South Dakota, 2000.

5.2 Forcing Data

5.2.1 Validation

Surface temperature measurements have been conducted at the Samoylov research station over the period from 28th August 2002 to 07th July 2009 (see Chapter 4.4 for details). This observational data from the ground was compared to the satellite product MODIS LST, which was used to force the model with land surface temperature data. The time series of surface temperatures from Samoylov Island is the only one available in the study region, so that validation of the temperature forcing data is restricted to this site.

The result of the comparison is shown in Fig. 11. The average deviation between MODIS LST and in-situ measured surface temperature resolved by months show a significant cold bias of up to -5 °C of the MODIS LST product, especially for the winter months. On the other hand, a warm bias is observed in the summer months. When the gaps in the MODIS LST time series are filled by ERA interim model data (Chapter 4.2.2), the average

deviations decrease significantly and the strong winter cold-bias is moderated. For the annual average, a slight cold bias of -0.8 °C remains (Fig. 11).

The validation of the temperature forcing with measurements on Samoylov Island suggests that the merged time series of MODIS LST and ERA is in satisfactory agreement with in-situ measurements, while stronger deviations occur when only MODIS LST is used.
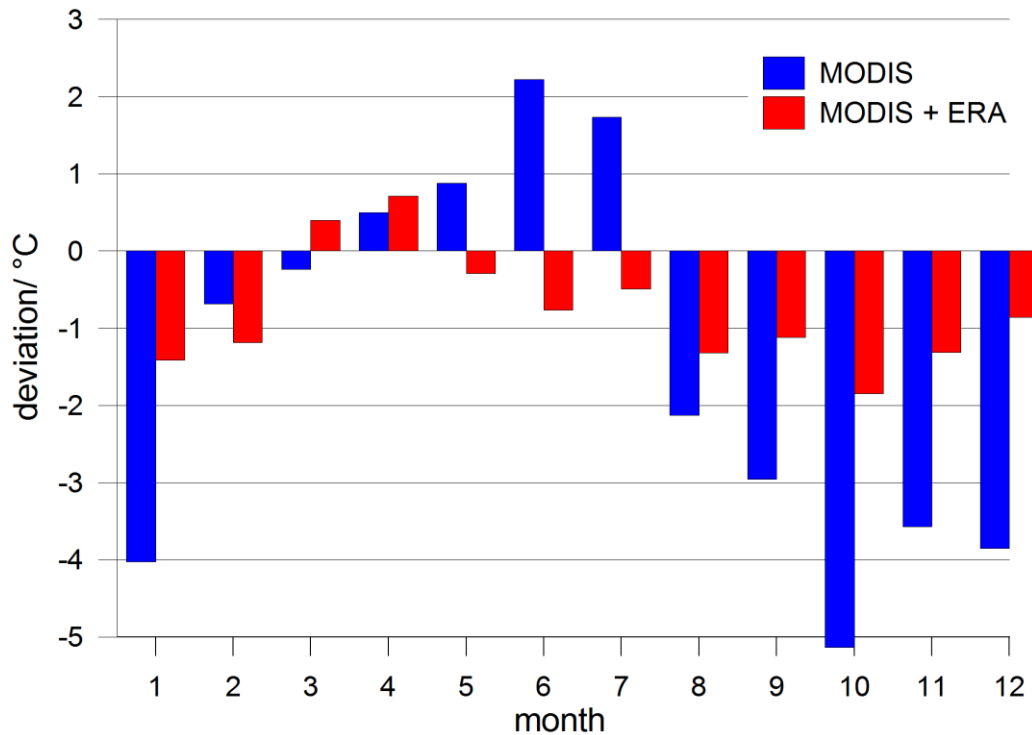
Fig. 11: Average deviations of MODIS LST minus ground-measured land surface Temperature and MODIS LST with ERA minus ground-measured land surface Temperature for each month of the year.

As for surface temperatures, only point measurements on Samoylov Island are available for snow depth. A comparison between the GlobSnow SWE derived snow depth and in-situ measured snow depth is presented in Langer et al. (2013), who found a good agreement, generally within 5 to 10 cm, with a few larger deviations for single years (see Appendix Fig. 29). Furthermore, the start and the end of the snow cover period is accurately represented.

5.2.2 Spatial distribution in the Lena River Delta

In this chapter the spatial distributions of the averages of snow depth, duration of snow cover and Land Surface Temperatures are presented to help interpret the modeled spatial

pattern of the ground thermal regime and distribution of soil temperatures throughout the Delta. The averages are calculated for the modeling period.

Average LST

Fig. 12 shows the calculated mean of the MODIS LST data for each grid cell for the time series from 2002 to 2013 that was used as forcing data for the model. The coldest average land surface temperatures of around -17.3 to -16 °C are measured for the northwestern part of the delta, approximately where Arga Island is located. An average LST of around -15 to -16 °C extents over most parts of the delta. Grid cells around the main channels show 1 to 4 °C higher surface temperatures, with a high gradient over short distances. The peninsula in the southeast that seems to protrude into the delta is not part of the delta and was not subject to modeling of permafrost temperatures, but was included in the map due to practical reasons. Also a narrow strip in mountainous hinterland south of the delta has been included.
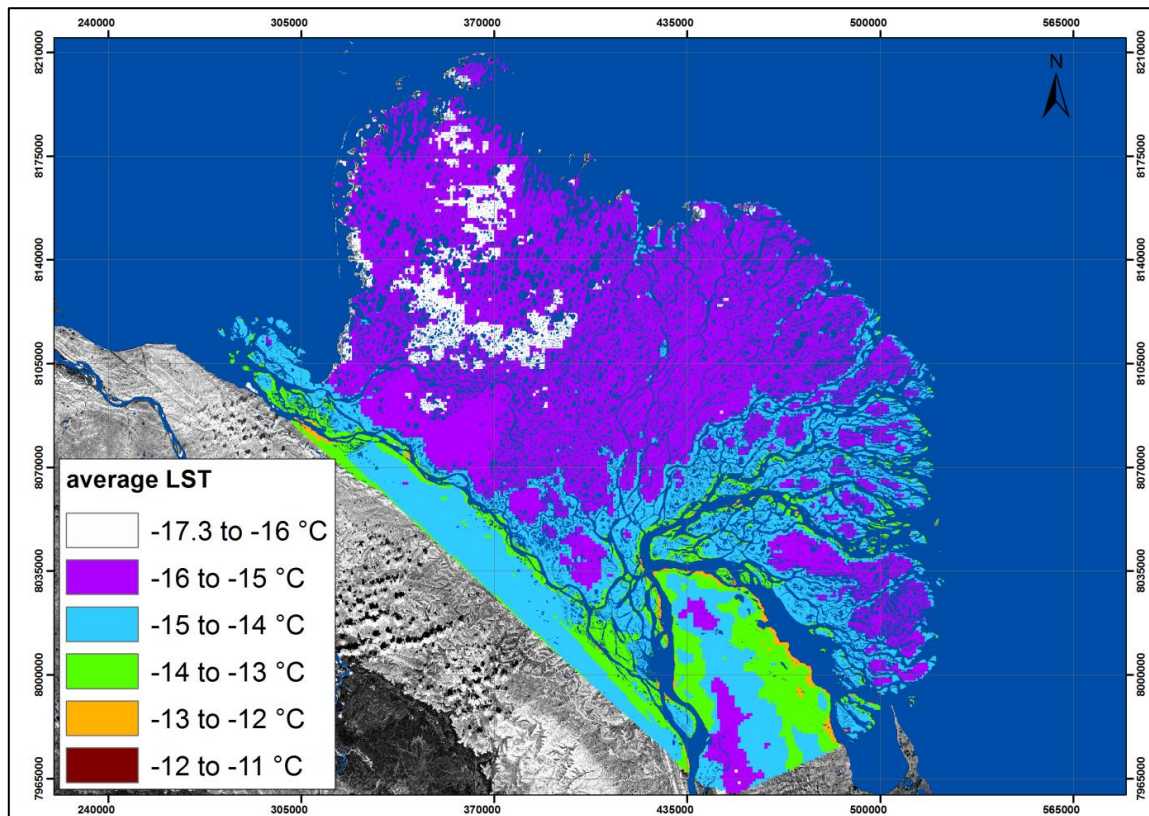
Fig. 12: Distribution of the mean Land Surface Temperatures from MODIS, averaged over the model period. UTM zone 52N. Base map and water masks are according to Chapter 5.1.1

To get a more detailed picture of the seasonal pattern of the satellite-measured land surface temperature, the averages for both the three winter months December, January and February and for the summer months June, July, August were calculated for every grid cell with the data of the modeling period.

In Fig. 13 the distribution of average winter temperatures is not strongly different from the all-season-mean. Here, coldest temperatures group in the northwestern part of the delta with temperatures as low as -37.5 °C, while around 70 percent of the grid cells feature an average between -36.0 and -34.5 °C. With up to -33 °C, average winter LST is slightly warmer in the vicinity of the river channels as well as in a thin fringe at the coastline.

Fig. 13: Distribution of mean Land Surface Temperatures from MODIS for the three winter months December, January and February, averaged over model period. UTM zone 52N. Base map and water masks are according to Chapter 5.1.1

For the three selected summer months the Land Surface Temperature distribution shows a significant range on the order of 5 K (Fig. 14). The lowest summer average temperatures of 4 to 5 °C are found along the coastline of the northwestern part of the Lena Delta. This is an opposite pattern compared to winter means. The summer mean gradually increases from North to South from around 4.5 to 8 °C. Close to the river channels in the southern part of the delta, grid cells with the highest summer mean temperatures of more than 9 °C are concentrated.

In a few areas, the summer pattern of the temperature distribution is different compared to the all-season and winter averages. Parts of the third terrace in the south and southwest of the delta show relatively cold temperatures in the all-season and the winter averages, while they feature relatively warm grid cells in the summer distribution. Also the land

surface temperatures on the Arga-Island are relatively higher in the summer while they are one of the lowest in winter and the all-season averages. Such patterns could be related to albedo or moisture effects in summer.
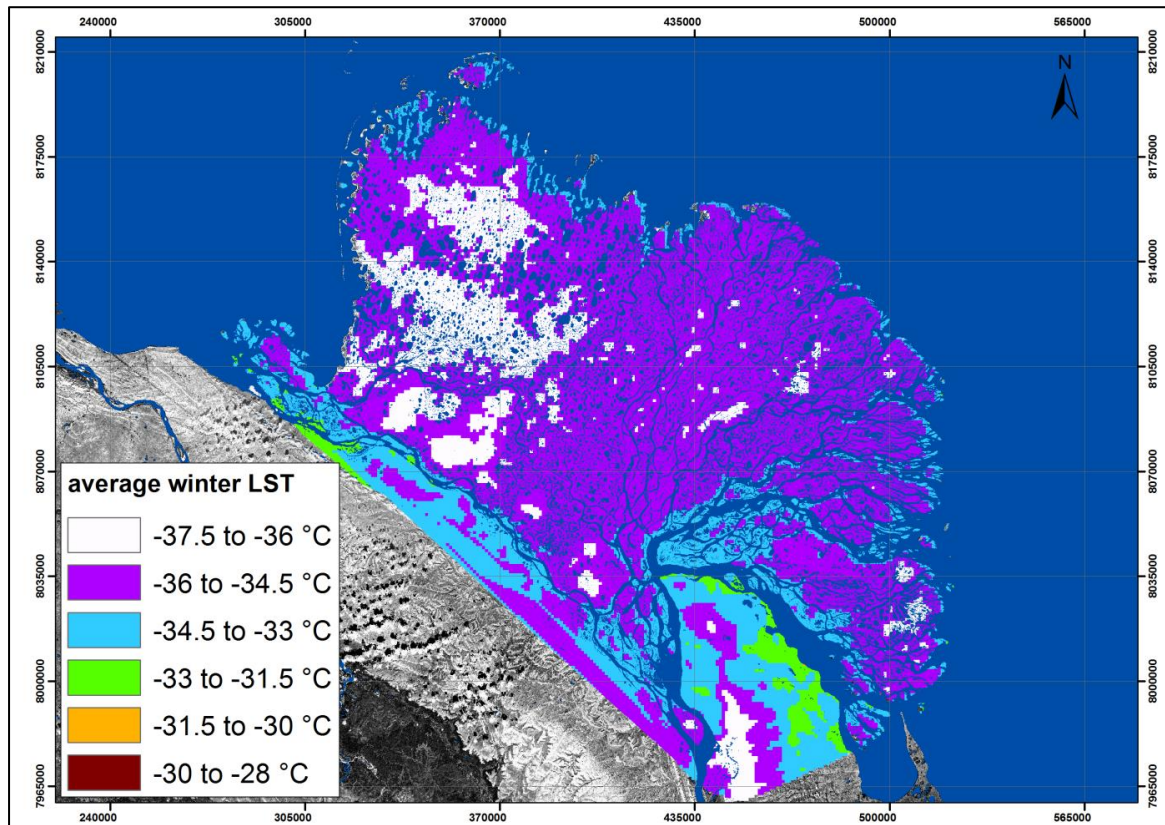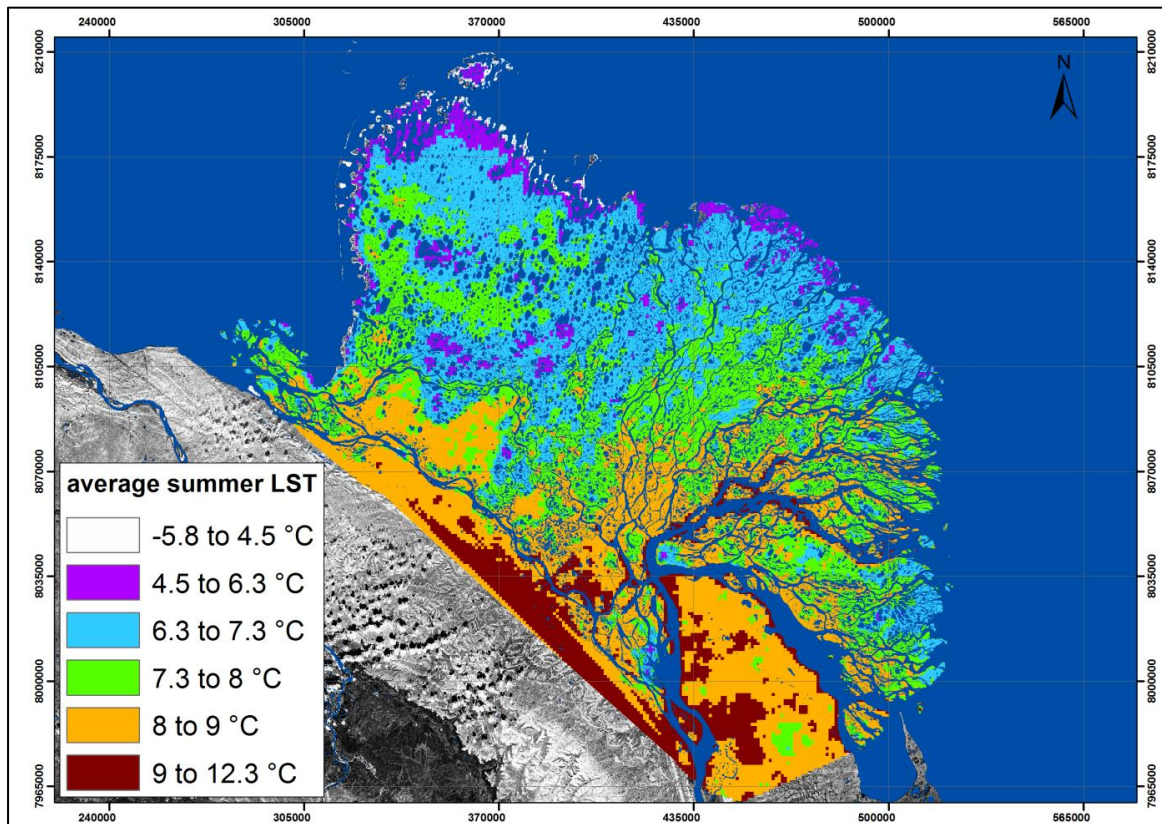

Fig. 14: Distribution of mean Land Surface Temperatures from MODIS for the three summer months June, July and August, averaged over the model period. UTM zone 52N. Base map and water masks are according to Chapter 5.1.1

In Fig. 15, the distribution of the annual average temperatures inferred from the MODIS LST plus ERA time series is shown for the delta. Here, in the mean 3 to 4 °C warmer temperatures are observed, while the spatial distribution has a similar pattern as for the Average MODIS LST only (Fig. 12). Generally, a northwest-southeast gradient of temperatures and a thermal influence of the river channels is visible in this average temperature distribution of the Lena River Delta. The coldest patches with about -14 to -14.5 °C are found in the northwest part of the delta, mostly where Arga-Island is located. Gradually warmer temperatures of -13.5 to -14 °C stretch over the largest part of the delta and cover the whole western and center parts of the delta. The warmest average temperatures are found for the eastern and southeast part, especially where the largest main river channels, Bykovskaya and Trofimovskaya, run. Here, average temperatures are -13.5 to -13 °C, and in some areas very close to these river channels even patches of -12.5 °C in average temperature are calculated. Also along the Olenyokskaya river channel this temperature distribution is observed. A fringe of very warm temperatures is

calculated for the coastline ranging from -13 °C in the east to larger than -12.5 °C in the west and northwest.
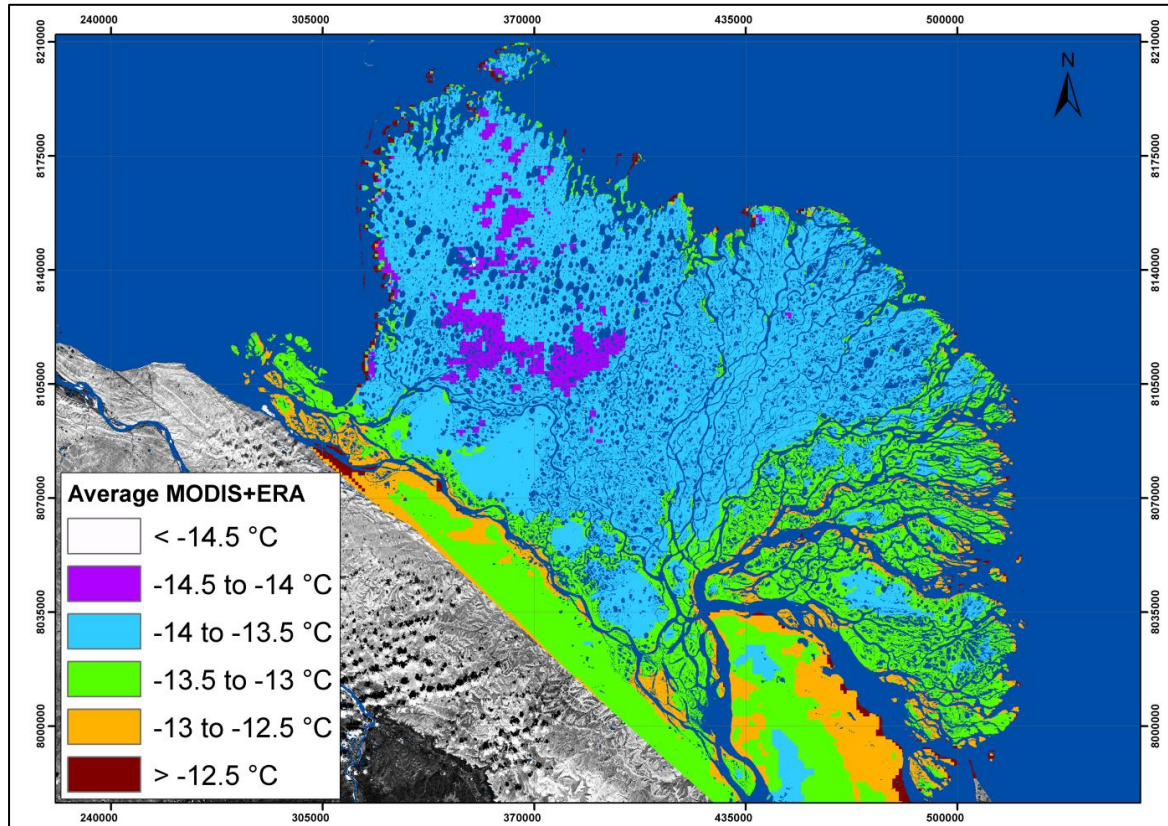
Fig. 15: Distribution of the MODIS LST plus ERA time series, averaged over the model period. Projected to UTM zone 52N. Base map and water masks are according to Chapter 5.1.1.

Averages of Snow depth and Snow Melt

Fig. 16 shows the average snow water equivalent distribution over the Lena River Delta. The mean is calculated from the GlobSnow SWE data series from 2002 until 2013, averaging over every date where snow is present during the course of the year. Unsufficient data quality of the product near the coastline is the reason for wide areas not to be included into to model calculation. The SWE is converted to snow depth by multiplying with a factor of 5, assuming that the density of snow is 200kg m^{-3} for this region (following Langer et al. 2013). The mapped averages reveal a significant west-east gradient of snow depth, with largest values in the southwest area of the delta of more than 40 mm snow water equivalent, i.e. around 20 cm of snow height. Lowest values are found in the most eastern part of the delta with less than 30 mm SWE. A slight continentality gradient can also be discerned, with values getting lower towards the coastline.
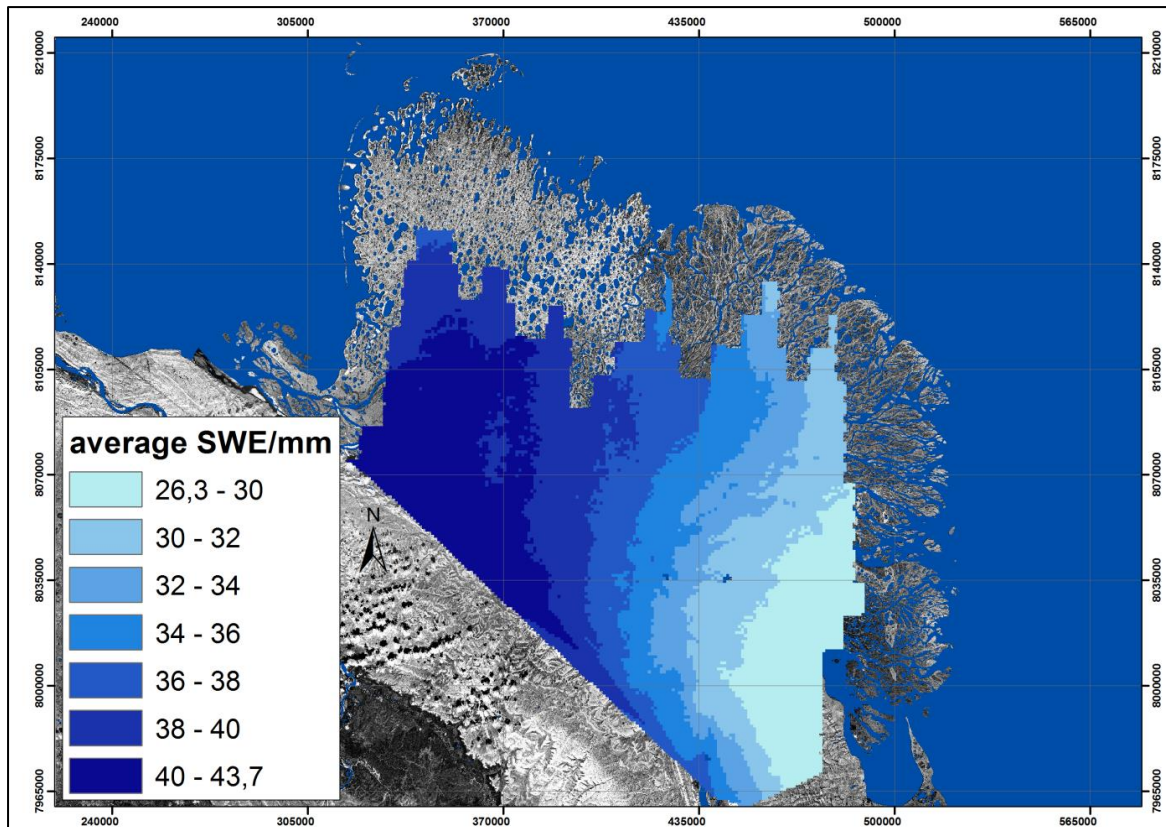
Fig. 16: Distribution of average snow water equivalent from GlobSnow, averaged over the model period. The higher spatial resolution of the grid cells is achieved by using the MODIS snow extent product for downscaling. UTM zone 52N. Base map and water masks are according to Chapter 5.1.1

Another important factor for permafrost distribution and permafrost temperatures is the length of the snow covered season. Therefore the time series for MODIS snow extent product was used to calculate the average end of the snow covered period with a daily resolution. This procedure also enhances the resolution of the GlobSnow SWE data from 25x25km to 1x1km (Chapter 4.2.3).

Fig. 17 shows the spatial differences in the average day of melt throughout the delta, with a north-south gradient indicating earlier snow-free conditions in the south. Furthermore, areas in the center of the delta melt out earlier, which could be related to continentality. Probably this effect is also coupled to the active river channels, transporting warmer water from the south and warming up areas close to the main river arms earlier than the rest of the delta. Here, the earliest snow-free grid cells appear on average around days 110 to 120 of the year, which is from 20th to 30th of April. The latest melt occurs around days 160 to 170, i.e. 9th to 19th June, especially in the northwestern part of the delta. This correlates with relatively cold Land Surface Temperatures (see Fig. 15 and 12), a relatively high snow depth (see Fig. 16) and a larger distance from active river channels, whereas the earliest melt in the south east correlates with higher LST, relatively low snow depth and the proximity to main river channels.

Fig. 17: Average day of melt throughout the delta, indicating the length of snow cover in spring, from the MODIS snow cover product, averaged over model period. UTM zone 52N. Base map and water masks are according to Chapter 5.1.1

5.3 Model results

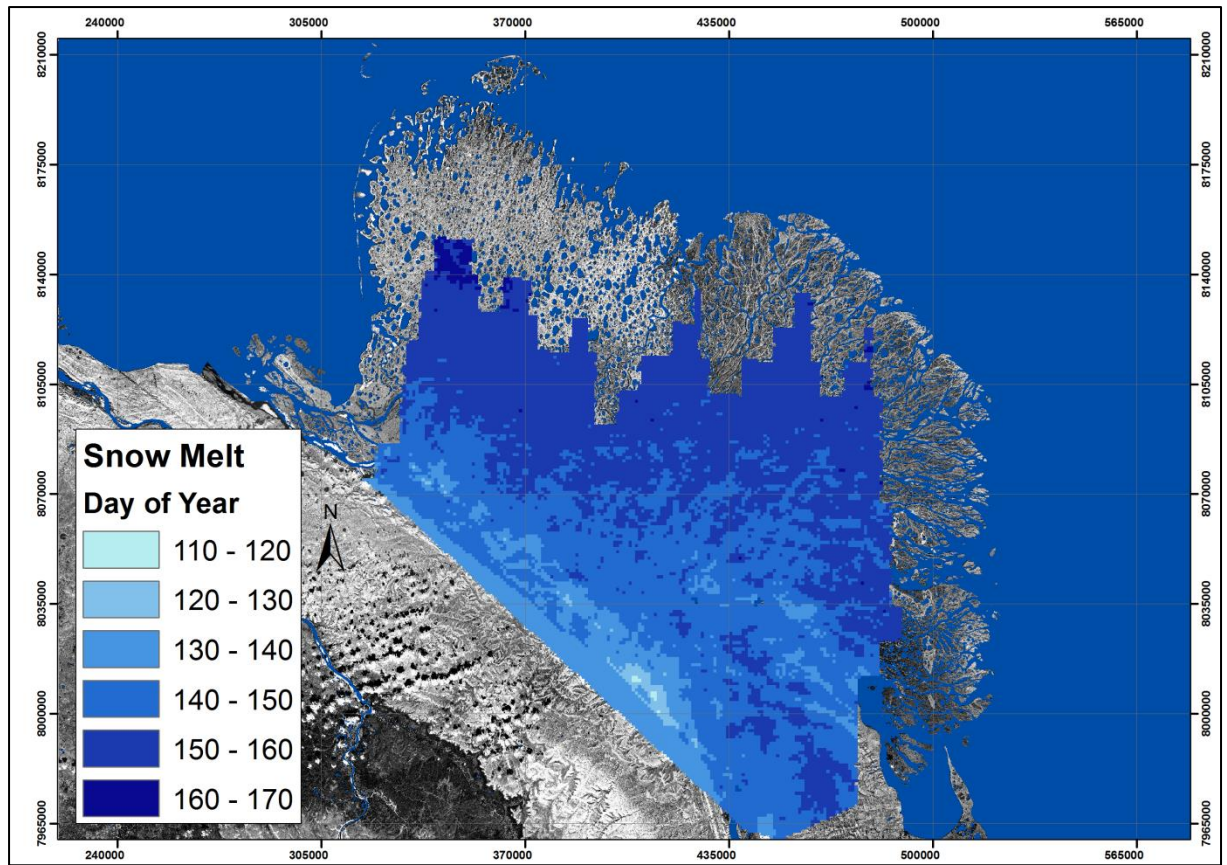The modeled period ranges from 01.08.2002 until 01.09.2011. Longer times series could not be performed because of unavailability of the GlobSnow SWE product after 2011 and the unavailability of complete MODIS products before 2002. As a result of low quality data of the GlobSnow SWE product for coastal areas, large areas of the delta had to be excluded from the modeling.

Two model runs were performed, one using MODIS LST only as temperature forcing, and one with ERA-interim integrated in the MODIS LST time series. Only the latter model run was used to further validate modeled ground temperatures at different sites of the delta (Chapter 5.3.2). The model results without ERA integration are only shortly presented and discussed, since a comparison of measured soil temperatures at 1 an 2 m depth from *Samoylov* Island (Chapter 5.3.2) and modeled temperatures for corresponding depths from the grid cell where Samoylov is located, showed 2 to 3 °C too cold temperatures calculated by the model, which is most likely related to the cold bias of the MODIS LST forcing data (Chapter 5.2.1). Due to significantly better performance (Chapter 5.3.2), only the model run using MODIS plus ERA data as forcing is analyzed in detail.

5.3.1 Distribution of the ground thermal regime

5.3.1.1 Model outputs for MODIS LST as forcing data

Fig. 18 shows the average of modeled temperatures for one meter depth for the modeling period from 2002 to 2011. Highest temperatures of around -9 to -11°C are modeled for grid cells close to the three main channels of the delta. Here, the influence of warm river water from the south is clearly visible in the nearby ground. These grid cells entirely belong to the first river terrace floodplain, as defined by Langer et al. (2013) that is a subclass of the first stratigraphic class.

The coldest ground temperatures from -13 to about -14.5 °C are modeled for central parts of the islands of the third river terrace as well as for eastern and northeastern parts of the first river terrace. In between and for the center of the delta, medium cold temperatures of -12 to -13 °C are modeled. The temperature distribution in the ground is strongly coupled to surface temperatures and snow distribution in winter, so these coldest spots can be explained by thin snow cover (see map of average snow depth).
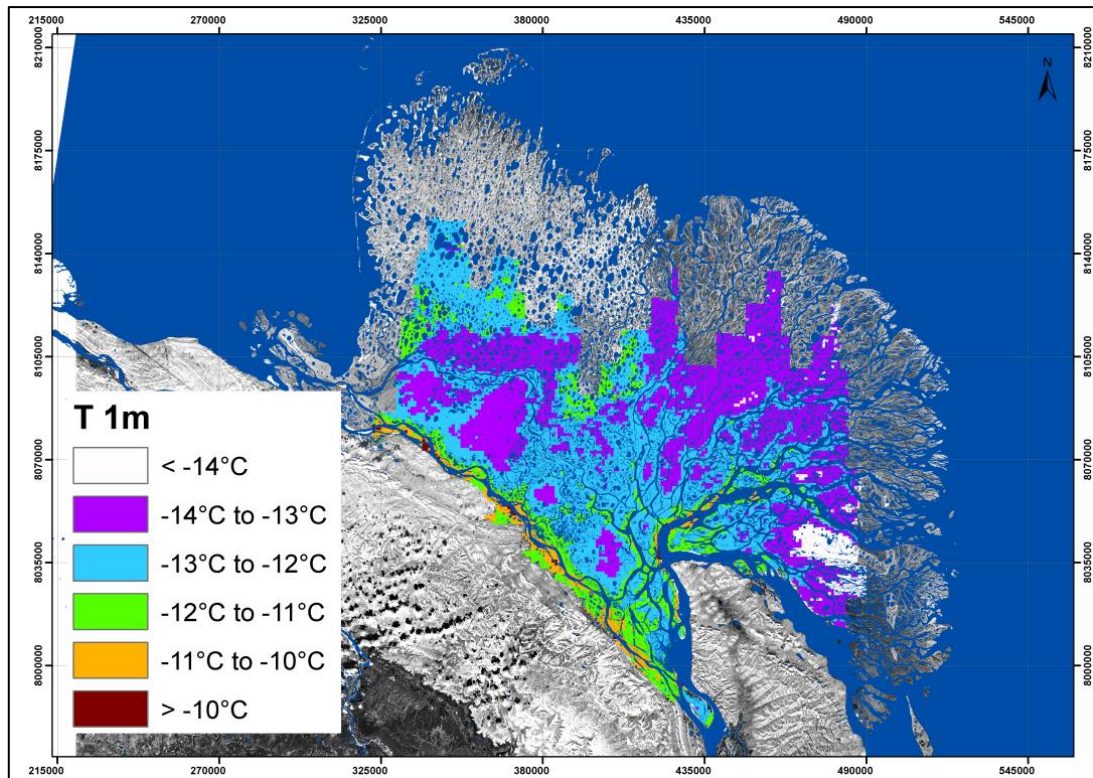
Fig. 18: Averaged permafrost temperatures from 1m depth with MODIS LST only. The averaged period is the whole modeling period from 2002 to 2011. UTM zone 52N. Base map and water masks are according to Chapter 5.1.1Peter et al. 2014a.
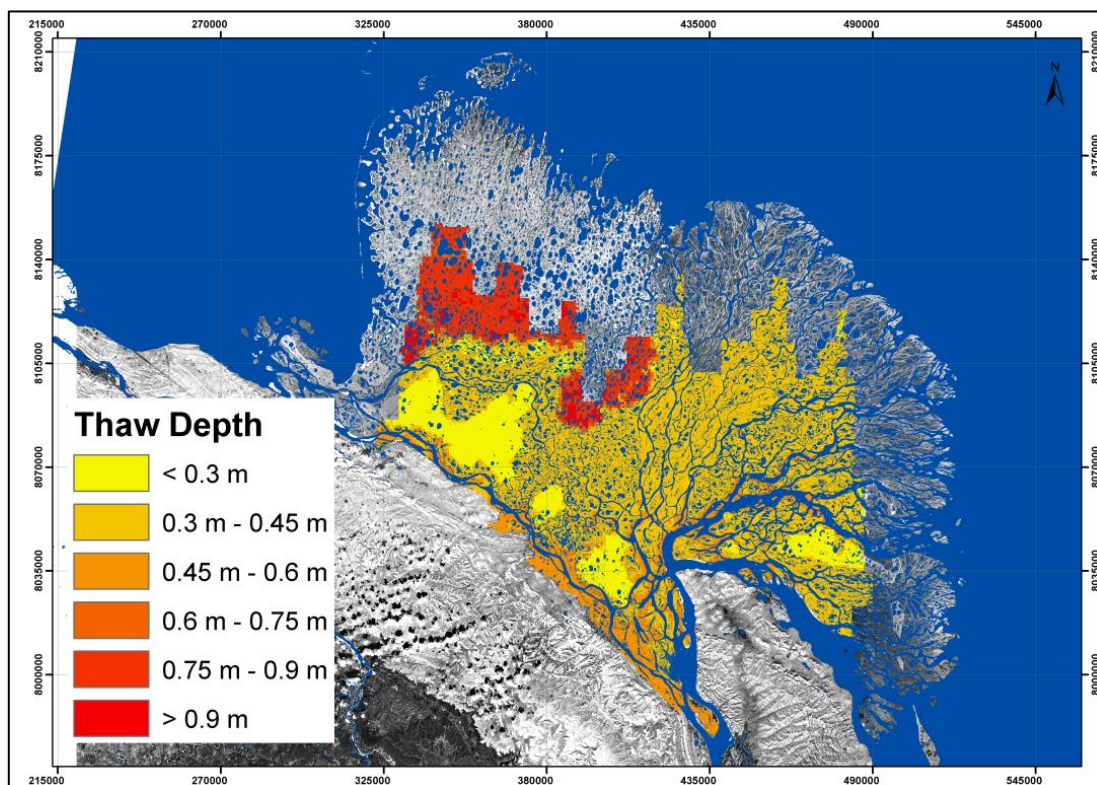

Fig. 19: Averaged thaw depths over model period with MODIS LST only. UTM zone 52N. Base map and water masks are according to Chapter 5.1.1.

In Fig. 19 annual maximum thaw depths, averaged over the nine year modeling period, are displayed. Here, the soil stratigraphy is strongly visible through the thaw depths. There is a very low thaw depth in the regions south and southwest of the delta and on one island in the east of about 30 cm or less. These regions are entirely part of the third old river terrace, which is also characterized as class three for the model. The deepest thaw depths are modeled for an area northwest in the delta of down to 100 cm. If this area is compared to the stratigraphy map or the terrace map of the Delta, it is obvious that these areas mostly belong to the second terrace or second stratigraphic class of the model. Medium thaw depths ranging from 45 cm to 80 cm are modeled for the rest of the delta, which is part of the first river terrace and first stratigraphic class. That means active layer thicknesses are more dependent on the composition and character of the ground material, than on surface temperatures or snow distribution.

5.3.1.2   Model outputs MODIS plus ERA data

To improve the time series of forcing data, the data gaps of the MODIS LST have been filled with available ERA-interim data (Chapter 4.2.2) which has a significant effect on the modeled results.

In Fig. 20 permafrost temperatures for one meter depth are presented in a 9-year average. Warmest mean permafrost temperatures are modeled for parts of the second terrace in the northwest and for the flanks of the Olenyoskaya river channel in the southwest of the delta that discharges to the west. Here, average 1m-permafrost temperatures of -8.3 to -10 °C are mapped. Medium cold temperatures of -10 to -11 °C are mapped for the center of the delta and thus large parts of the 1st stratigraphic unit. The more to the east and to the coastline of the 1st stratigraphic class, colder 1m-temperatures of down to -12.5 °C are calculated. For the western half of the delta these coldest average temperatures are only modeled for parts of the 3rd stratigraphic unit with -11 to -11.5 °C. This distribution of average 1 m-ground temperatures shows a clear influence of not only the stratigraphic units but also of the average snow distribution patterns and length of the snow cover period (Chapter 5.2.2).
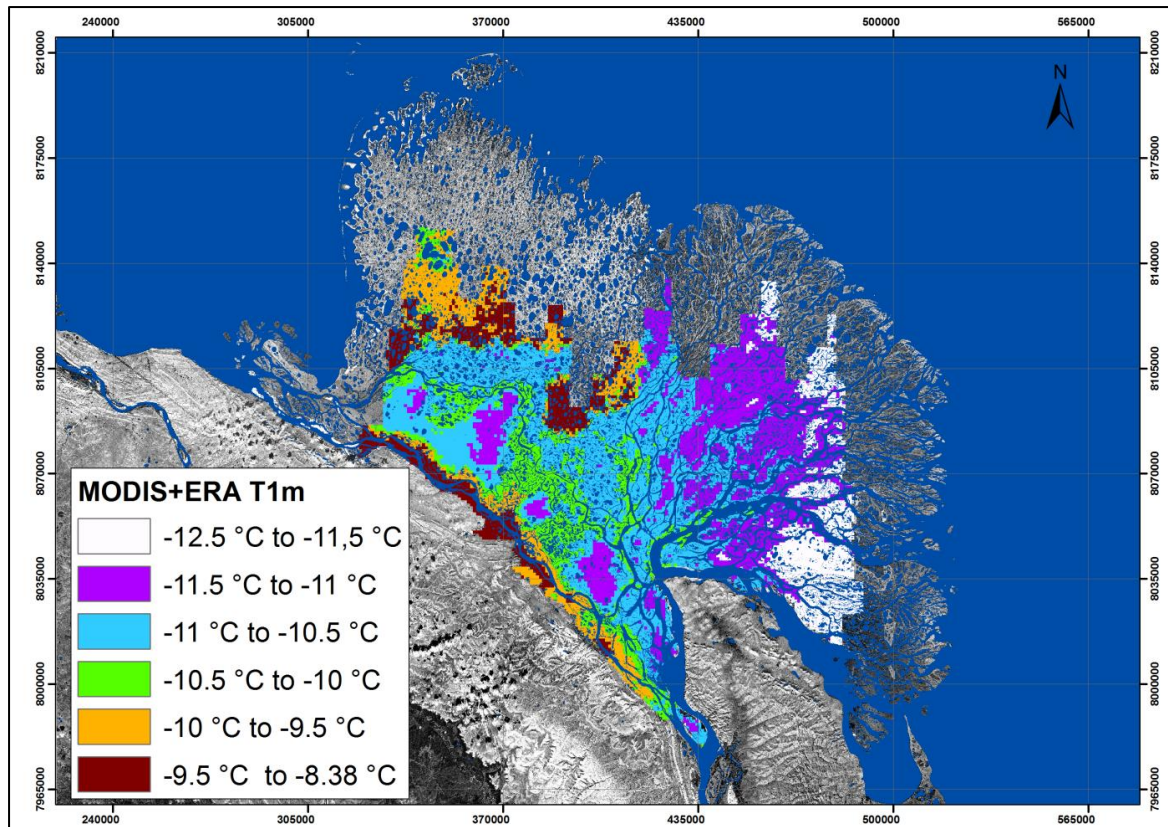
Fig. 20: Distribution of modeled mean ground temperatures in 1 meter depth from model runs with ERA-interim product integration, averaged over model period from 2002 to 2011. UTM zone 52N. Base map and water masks are according to Chapter 5.1.1

For the average distribution of thaw depth throughout the delta a similar pattern as for model forcing without integration of the ERA-interim data could be observed (Fig. 21). This pattern suggests an even stronger correlation of stratigraphic class and thaw depth than for the 1-m ground temperature distribution. Generally, on average about 5 to 10 cm smaller thaw depth were calculated for the whole delta, which is probably connected to the ERA integration, resulting in colder summer temperatures (Chapter 5.2.1). Average maximum thaw depths of 20 to 30 cm were modeled for the 3rd stratigraphic unit, while deepest average maximum thaw depths of 70 to up to 93 cm are assigned to the 2nd class. For the 1st stratigraphic class, medium averages of 30 to 70 cm are modeled. The 1st class shows the most variability in thaw depths as it also features relatively low thaw depths in the central, northern and eastern delta and relatively high thaw depths near the main river channels and in the southern delta. In the northernmost area of the 1st class a transition to shallower thaw depths (as low as for the 3rd terrace) is visible. This can be explained as an influence of the average snow distribution and average surface temperatures in summer (Chapter 5.2.2).
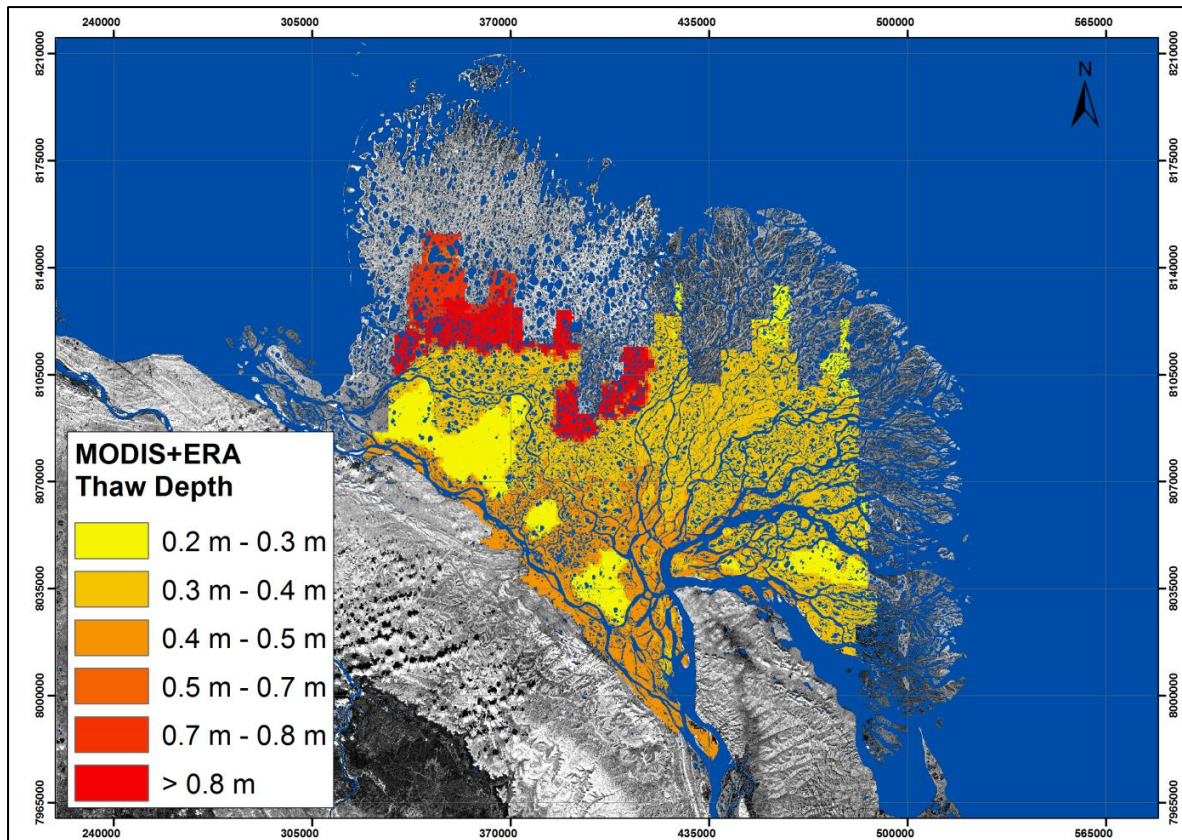
Fig. 21: Modeled distribution of average maximum thaw depth throughout the delta with ERA-interim product integration, average from the model period from 2002 to 2011. UTM zone 52N. Base map and water masks are according to Chapter 5.1.1

5.3.2 Validation

The model results were validated both for ground temperatures and thaw depth for seven different field sites, *Samoylov, Kurungnakh, Mitte, Ozean, Jeppiries, Arga, Sardagh*, where in-situ data had been collected during the modeling period (see Fig. 22). The technical details and methods how the observational data were collected are explained in Chapter 4.4. With this data basis, all three stratigraphic classes are covered with at least two in-situ measurement sites, so that a spatially distributed validation of the model can be performed.
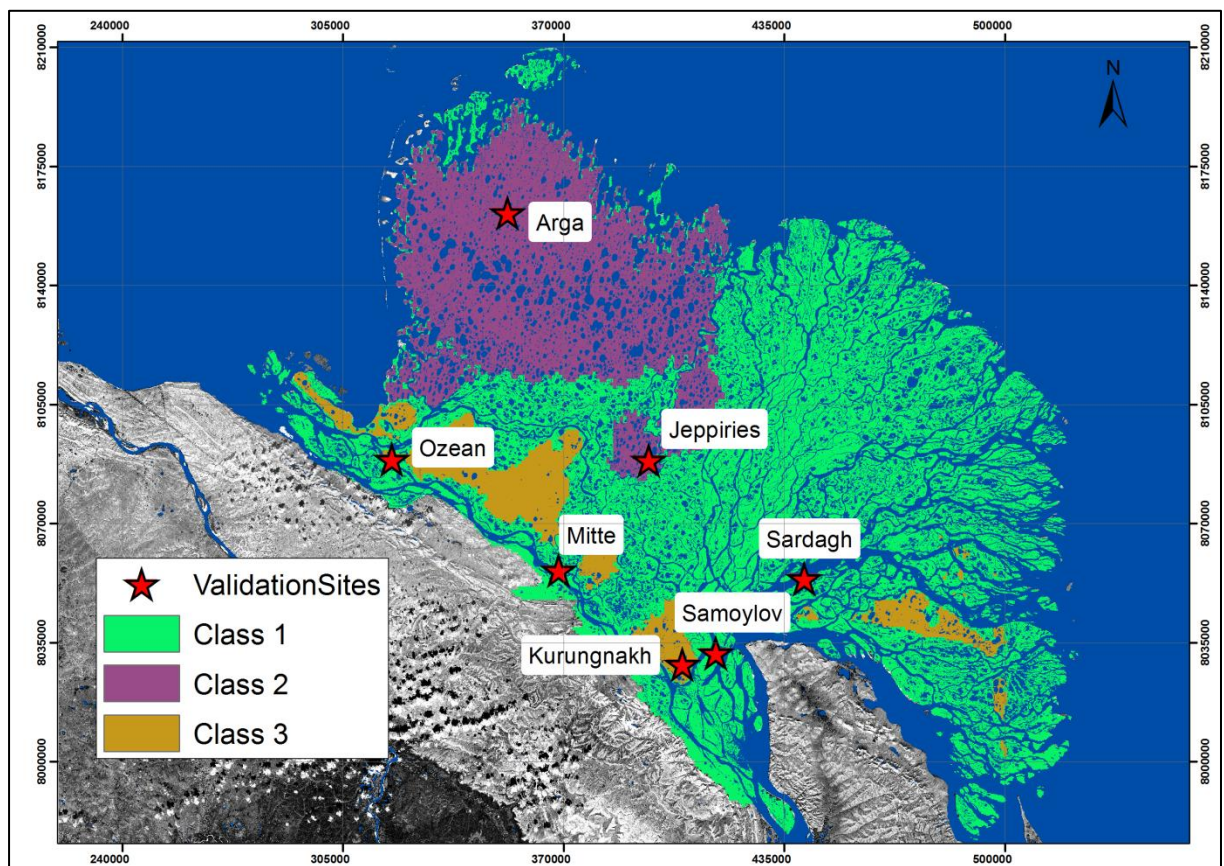
Fig. 22: Stations with ground-measured data used for validation of the model and their location on the stratigraphic units. UTM zone 52N. Base map and water masks are according to Chapter 5.1.1.

5.3.2.1 Validation of modeled ground temperatures

5.3.2.1.1 Stratigraphic Class 1

Samoylov

For the first stratigraphic class, validation data from the Samoylov Permafrost Observatory (N 72°22'12.0" E 126°28'51.9") (Fig. 23) were used to validate modeled ground temperatures for several depths and years using a 26m deep borehole (position: N 72°22'10.4", E 126°28'30.4").

Fig. 23: The old Samoylov Research Station, located on the first river terrace, respectively first class of model stratigraphy. (Photo by: AWI, Expedition Samoylov April 2011).

The comparison of soil temperatures was performed for two time slices, due to extended data gaps in the borehole data (Table 2). In 2006/2007, average temperatures agree within approximately 0.5 °C for temperatures at 1.75 m and 2.75 m depth. Until 2010/2011 a significant warming was found in the lower part of the borehole, while this warming is not observed at the sensor located at the surface (i.e. 0 m). The model does not represent this warming, with average temperatures more or less unchanged compared to 2006/2007. It is unclear whether the warming trend in the borehole is representative for the large scale ground thermal regime of Samoylov Island (as it is delivered by the modeling) or caused by local effects related to the particular setting of the borehole. In any case, the discrepancy cannot be explained in the framework of this thesis.

Table 2: Comparison of measured and modeled temperatures in 4 different depths and for 2 periods of time for the deep borehole on Samoylov Island.

Samoylov N 72°22'10.4'',E 126°28'30.4''			
Depth in m	**period**	**measured in °C**	**modeled in °C**
1.75	Sept 1 2006 - Sept 1 2007	-9.24	-9.8
2.75	Sept 1 2006 - Sept 1 2007	-9.2	-9.7
0	Sept 1 2010 - Sept 1 2011	-9.3	-8.6
0.75	Sept 1 2010 - Sept 1 2011	-6.4	-9.8
1.75	Sept 1 2010 - Sept 1 2011	-6.5	-9.8
2.75	Sept 1 2010 - Sept 1 2011	-6.6	-9.8

Mitte

At validation site 'Mitte' (N 72°33'56.9" E 125°03'52.3"), also in the first class, there is a borehole of 2.30 m depth instrumented with 6 sensors, providing hourly data from 16th Aug 2010 to 04th Aug 2011 (pers. comm., M. Langer). The borehole is located in a rather homogenous landscape (Fig. 24) and is thus well suited for validation of 1 km-scale model results.

Table 3: Comparison of measured and modeled temperatures for the 'Mitte' site, situated in stratigraphic class 1.

Site ,Mitte' N 72°33'56.9" E 125°03'52.3"			
Depth in m	**period**	**measured in °C**	**modeled in °C**
0.235	Aug 16 2010 - Aug 4 2011	-7.0	-7.2
0.735	Aug 16 2010 - Aug 4 2011	-7.3	-7.5
1.235	Aug 16 2010 - Aug 4 2011	-7.35	-7.6
1.735	Aug 16 2010 - Aug 4 2011	-7.4	-7.7
2.235	Aug 16 2010 - Aug 4 2011	-7.3	-7.8

Here a good agreement between measured and modeled yearly average temperatures is found. For all considered depths the modeled and measured temperatures agree within 0.5 °C or better (table 3). For this site a detailed comparison for the entire time series was performed for four depths (Fig. 25).

Fig. 24: Climate station at validation site ‚Mitte'. The borehole is located 50 to 100 m southeast of the climate station (Photo by J. Sobiech, 2011).
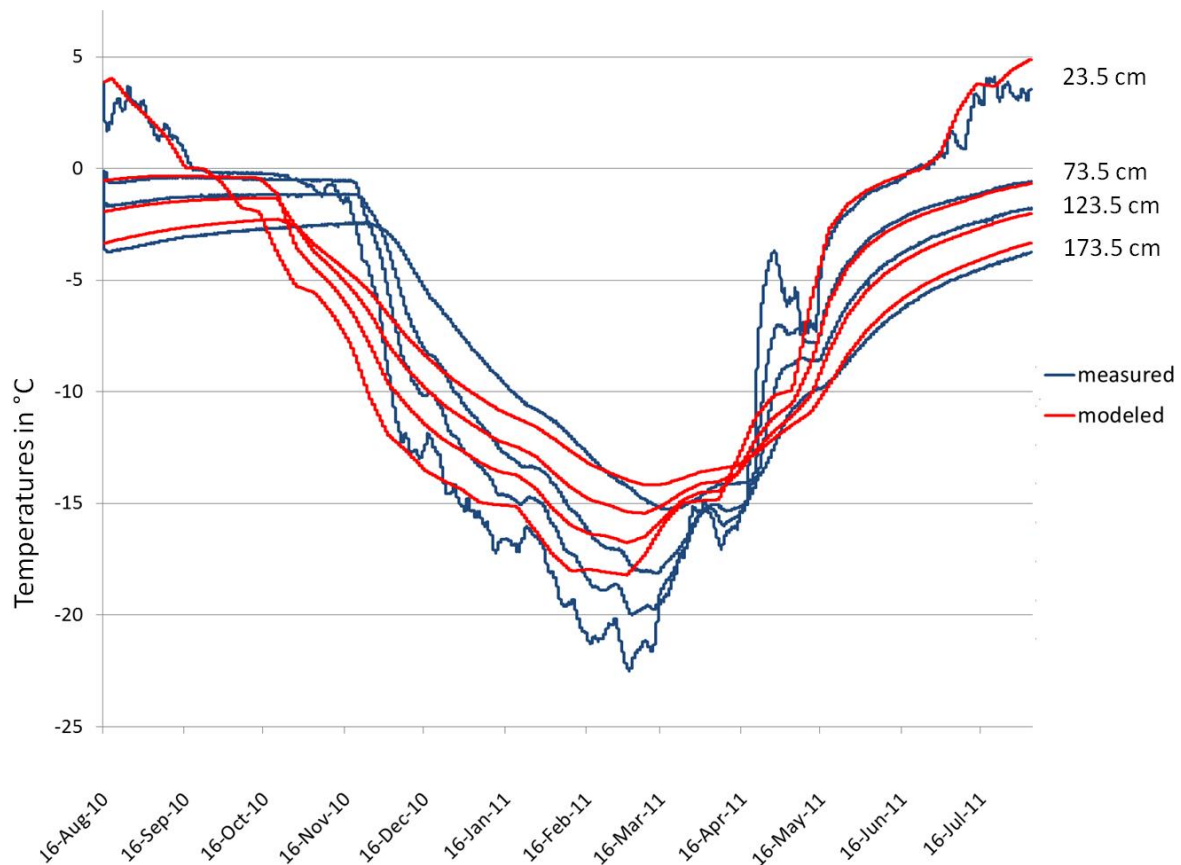
Fig. 25: Detailed comparison of measured and modeled temperatures for 4 depths for the site 'Mitte'.

During the summer months the measured and modeled values agree generally well within 1 °C. During fall, winter and spring significantly stronger differences are found, especially during the soil freezing period in fall (October/November) when modeled temperatures decrease to less than -5 °C. In reality temperatures are close to 0 °C for a

50

long period before decreasing sharply to even lower than modeled temperatures in mid-winter. In spring measured temperatures increase stronger than the modeled ones which could be related to infiltration of water from the melting snowpack into the ground, which is not accounted for in the model (see Westermann et al. 2013).

5.3.2.1.2   Stratigraphic Class 2

Arga & Jeppiries

For the second stratigraphic class there is no usable temperature data to validate the modeled ground temperatures.

5.3.2.1.3   Stratigraphic class 3

Kurunaghk

From July 10 2009 until Aug 20, 2010 there exists temperature data from a 4-m deep borehole (N 72°19'12.5" E 126°11'35.7") in an 'alas' depression on the island Kurungnakh (pers.comm, J. Boike). In this case, the installation of the borehole affected the surrounding soil thermal regime significantly during the course of the year. When reading out data in summer 2010, a small water filled depression, i.e. the initial stadium of a thermokarst thaw lake, had formed around the borehole. Still, the beginning of the data series most likely delivered ground temperatures unaffected by this pond. The 2-month-average temperature from July and August (10th July 2009 – 31st Aug 2009) shows -9.4 °C for the deepest sensor at 4 m. For the same period the modeled temperatures are -9.8 °C for this grid cell, and this within 0.5°C of each other (table 4).

Table 4: Comparison of measured and modeled ground temperatures for a borehole on Kurungnakh Island.

Borehole ‚Kurungnakh' N 72°19'12.5" E 126°11'35.7" (thermokarst affected)			
depth in m	period	measured in °C	modeled in °C
4.0	Jul 10 2009 - Aug 31 2009	-9.4	-9.8

Ozean

At the Validation Site 'Ozean' (N 72°49'20.1", E 123°30'45.0") which is also located on the third stratigraphic class, data are available from a 2.20 m-deep borehole for the period from 14th Aug 2010 to 16th Aug 2011(pers. comm., M. Langer). The surroundings of the site are homogeneous (Fig. 27).

For this period the permafrost temperature shows -8.7 °C in average at the bottom of the borehole at 2.20 m depth. 'Ozean' is located just ouside of the modeled area, so the closest modeled grid cell on the third stratigraphic class was used. Still, a satisfactory agreement between model results and measurements is achieved, with temperatures matching very well at 1.2 m depth and below (table 5).

Table 5: Comparison of measured and modeled ground temperatures. Note that the 'Ozean' site is outside the modeled area and the nearest grid cell of class 3 was used instead.

Ozean N 72°49'20.1", E 123°30'45.0"			
depth in m	period	measured in °C	modeled in °C
0.2	Aug 16 2010 - Aug 16 2011	-8.9	-7.8
0.7	Aug 16 2010 - Aug 16 2011	-7.4	-8.1
1.2	Aug 16 2010 - Aug 16 2011	-8.2	-8.2
1.7	Aug 16 2010 - Aug 16 2011	-8.3	-8.4
2.2	Aug 16 2010 - Aug 16 2011	-8.7	-8.5

Fig 26: Climate Station at site 'Ozean'. The borehole is located 5 m next to the station, plastic pipe visible in the background. Photo by J. Sobiech 2011.

5.3.2.1.4   Sardagh

A 100 m deep borehole located in homogeneous surroundings (Fig. 27) has been set on Sardagh (N 72°19'12.6", E 127°14'29.4"), providing data from 17.08.2009 until 18.08. 2010 (pers. comm., J. Boike). Sardagh stands outside of the classification, since it is old intrusive bedrock with a normal deltaic/fluvial sediment cover, but doesn't feature the same ice contents like the third terrace and is not as deep developed as the surrounding ground. Superficially and in terrace-height it can be assigned to the third stratigraphic class, but not in the contents. Sardagh has colder ground temperatures compared to the previous sites, which are very well reproduced by the modeling, despite of the differences in the soil stratigraphy. For all depths measured and modeled average ground temperatures agree within 0.5°C (table 6).

Table 6: Comparison of measured and modeled ground temperatures for the ‚Sardagh' site.

Sardagh N 72°19'12.6", E 127°14'29.4"			
depth in m	period	measured in °C	modeled in °C
0.75	Aug 17 2009 - Aug 18 2010	-10.6	-10.5
1.75	Aug 17 2009 - Aug 18 2010	-10.5	-10.6
2.75	Aug 17 2009 - Aug 18 2010	-10.4	-10.7
3.75	Aug 17 2009 - Aug 18 2010	-10.4	-10.8

Fig. 27: Site of the 100-m–borehole on Sardakh Island. Picture: AWI.

5.3.2.2 Validation of modeled thaw depth

5.3.2.2.1 Stratigraphic Class 1

Samoylov

A series of thaw depth measurements from 2002 until present is available in the form of a CALM-grid site (N 72.369775 E 126.480632). It features 150 measurement points in a grid of 18x27.5 m. Values from Boike et al. (2013) and Langer et al. (2013) show a mean of about 0.5 m depth of active layer on Samoylov island, measured each year in August at the same polygon-site. In total, the data from 8 years from 2002 until 2010 were used to calculate the mean of maximum measured thaw depth. In the year 2004 there was no measurement made. Fig. 28 shows the comparison of the range of measured thaw depths and the annual maximum modeled values for every year. This shows an overall good agreement of modeled thaw depths with measured values for this grid cell. The modeled values are always within the range of the measured values which represent the significant spatial variability of the site. Especially in the second half of the time series, the inter-annual variations of the thaw depth are to a large extent reproduced.
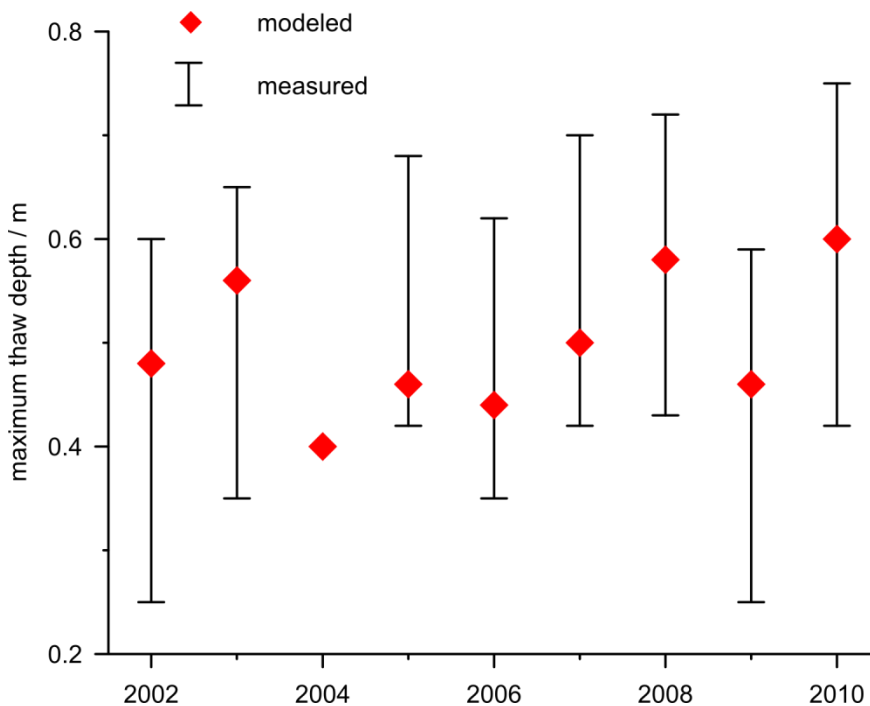

Fig. 28: Comparison of in-situ measured thaw depths from CALM-site and modeled maximum average thaw depths from the grid cell which is located over the CALM-site. Table of values shown in appendix.

Mitte

One thaw depth measurement was performed at the 'Mitte' site (N 72°33'56.9" E 125°03'52.3") during the model period. On 16 August 2010, 60 cm of thaw depth were measured (pers. comm., M. Langer) which agrees within 2 cm with the thaw depth calculated by the model for the same day (Table 7). In the same year, the maximum modeled thaw depth was 65 cm, and the sensor of the temperature chain at 73 cm depth showed always negative temperatures (see above). This suggests that the annual maximum thaw depth is reproduced within at least 5 to 10 cm.

Table 7: Comparison of measured and modeled thaw depth for site ‚Mitte‘.

Thaw Depth ‚Mitte‘ N 72°33'56.9" E 125°03'52.3"		
time	measured in m	modeled in m
Aug 16 2010	0.6	0.58

5.3.2.2.2   Stratigraphic Class 2

Arga

For validation of thaw depths of the second stratigraphic class a single point measurement on Arga-Island (N 73°29'39.2" E 124°22'33.1") is available. On the 11th Aug 2010 a thaw depth of 90 – 100 cm was measured (pers. comm., M. Langer). Since this point is located outside the modeled area the closest model grid cell classified as class 2 was used for validation. The agreement between model and measurement is still excellent, with a modeled thaw depth of 0.96 m for 11th August 2010.

Table 8: Comparison of measured and modeled thaw depths for the validation sites Arga and Jeppiries.

Thaw Depth Arga N 73°29'39.2" E 124°22'33.1" & Jeppiries N 72°51'14",E 125°50'22"			
	Time	measured in m	modeled in m
Arga	Aug 11 2010	0.9 – 1.0	0.96 (for closest grid cell in 2nd class)
Jeppiries	Jul 23 1998	0.7	0.69 – 0.96 (for all modeled years)

Jeppiries

During the LENA Expedition 1998 thaw depth measurements were taken at Jeppiries Island, part of the second terrace in the center of the delta. Here near the Lake Yugus-Jie-Kuyele (72°51'14"N, 125°50' 22" E) a thaw depth of 0.7 m has been measured on 23rd July 1998 (Rachold & Grigoriev 1999). As for the year 1998 there are no modeled temperatures (model period starts 2002), the values of every July 23rd in the modeling period were checked for this grid cell. Depending on the year, the model calculated a thaw depth of 0.62 to 0.96 m for the grid cell of 'Lake Yugus-Jie-Kuyele'. The measured thaw depth of 1998 lies within the range of the modeled thaw depths for the same day of the year.

5.3.2.2.3   Stratigraphic Class 3

Kurungnakh

For Kurungnakh Island 9 thaw depth measurements conducted during the Lena Delta Expedition in 2013 (pers. comm., S. Niemann) were used to validate thaw depths of three model grid cells located on this island. They were taken in approximate distance or directly by a thermokarst lake 'Lucky Lake' (N 72.294726 E 126.159457) at the beginning, middle and again at the end of the Expedition, but still may not represent the maximum thaw depths of year 2013. Since the dates of measurement are not within the model period, they cannot be directly compared. For this reason, the range of modeled thaw depths of the years from 2002 to 2011 is compared with the range of the thaw depths of 2013 in table 9. These measurements confirm the generally low thaw depth on the third terrace, with values between 10 and 30 cm. The model can more or less reproduce these low values, but the maximum thaw depths are generally a bit higher than the measured values in August. However, the agreement is still in the range of 10 to 15 cm.

Table 9: Ranges of measured and modeled thaw depths for 9 locations on Kurungnakh Island.

Thaw Depths ‚Kurungnakh' near Lucky Lake						
	Measured in m			**Modeled in m**		
Location around thaw lake ‚Lucky Lake'	July 14&15 2013	Aug 9&10 2013	Aug 26 2013	Average max thaw depth of all years	min. of all years	max. of all years
southern shore I	0.16	0.21	0.23	0.29	0.22	0.36
southern shore II	0.16	0.22	0.23	0.3	0.22	0.38
southern plateau	0.12	0.16	0.21	0.3	0.22	0.38
eastern plateau I	0.17	0.21	0.26	0.3	0.22	0.38

eastern plateau II	0.18	0.22	0.25	0.3	0.22	0.36
eastern plateau III	0.16	0.19	0.23	0.29	0.22	0.36
western plateau I	0.16		0.24	0.29	0.22	0.36
western plateau II	0.14		0.23	0.29	0.22	0.36
western shore	0.17		0.25	0.29	0.22	0.36

Ozean

For the 'Ozean' site one thaw depth measurement was performed on August 14 2010 during the Lena Delta Expedition 2010. Thus the location of this measurement point is not located in the modeled area the closest grid cell classified as class 3 was used for validation. The modeled thaw depth of 30 cm of the closest grid cell calculated for the same day is within 10 cm agreement to the measured value of 20 cm (pers. comm., M. Langer).

Table 10: Comparison of measured and modeled thaw depth for 'Ozean' site.

Thaw Depth ‚Ozean' N 72°49'20.1'', E 123°30'45.0''		
time	**measured in m**	**modeled in m**
Aug 14 2010	0.2	0.3 (closest grid cell to 'Ozean' on third terrace)

5.3.3 Sensitivity Analysis

To further investigate the performance of the model, a sensitivity analysis was run for the seven validation sites regarding the influence of the stratigraphic classes (table 11). For the grid cell of the Samoylov site, a more in-depth sensitivity analysis was made by Langer et al. (2013). Performing such work for the entire study region, i.e. more than 15,000 grid cells, would require significant computational resources and was not performed in the framework of this thesis.

Table 11: Sensitivity analysis focusing on the influence of the stratigraphic classes for the modeling. Temperatures in °C, cell nr = number of model grid cell, class = defined stratigraphic class for model, T1m = average temperature in 1 meter depth over entire modeling period, analogue for T2m and T10m, averageTD = average maximum thaw depth over all modeled years in meters.

	cell nr	class	T1m	T2m	T10m	averageTD
Arga	9064	1	-10,4	-10,4	-10,5	0,3
	9064	2	-8,9	-8,9	-9,0	0,9
	9064	3	-11,0	-11,0	-11,0	0,2
Jeppiries	26394	1	-9,8	-9,8	-9,9	0,4
	26394	2	-7,9	-7,9	-8,1	1,0
	26394	3	-10,5	-10,5	-10,6	0,2
Kurungakh	38300	1	-9,8	-9,8	-9,7	0,5
	38300	2	-7,7	-7,8	-7,7	1,2
	38300	3	-10,4	-10,4	-10,4	0,3
Mitte	30355	1	-8,5	-8,6	-8,7	0,5
	30355	2	-6,4	-6,4	-6,7	1,2
	30355	3	-9,4	-9,4	-9,5	0,3
Sardagh	36413	1	-10,3	-10,3	-10,2	0,5
	36413	2	-8,6	-8,6	-8,6	1,1
	36413	3	-10,7	-10,7	-10,6	0,3
Ozean	21032	1	-8,2	-8,2	-8,3	0,5
	21032	2	-6,0	-6,0	-6,2	1,2
	21032	3	-9,2	-9,3	-9,4	0,3
Samoylov	38004	1	-9,8	-9,8	-9,7	0,5
	38004	2	-7,8	-7,9	-7,9	1,2
	38004	3	-10,3	-10,3	-10,2	0,3

The results of this analysis reveal a clear influence of the stratigraphic definition not only on the thaw depths but also on the further temperature regime in several depths. The difference between the classes is at some points as large as 2.5 °C. If the model is forced with the different stratigraphic classes for one point, differences in thaw depths as large as

90 cm are calculated. The sensitivity analysis clearly demonstrates why the outline of the stratigraphic classes becomes visible in both modeled 1m- ground temperatures (Fig. 20) and thaw depths (Fig. 21).

6 Discussion

6.1 Evaluation of the results

For most sites, validation results indicate a model accuracy of 1°C or better for average annual ground temperatures and better than 10 cm for annual maximum thaw depths. However, for the borehole on Samoylov Island, significantly larger deviations than 1°C between measured and modeled annual average ground temperatures were found. These deviations occur at the end of the modeling period following a strong increase of ground temperatures in the borehole. Since ground temperatures close to the surface do not show the same increase, it remains unclear whether the observed warming and thus the deviations to the model result represent the behavior of the large-scale ground thermal regime on Samoylov Island or not. For the evaluation of the model accuracy and its potential to model changes in ground temperature over time, this is a highly crucial point which should be investigated in more detail.

The sparse measurements of ground temperatures within the delta confirm a spatial variability of at least 3 °C of annual average ground temperatures (Comparison site 'Mitte' and 'Sardagh', Chapter 5.3.2) within the Lena River Delta. The measured thaw depths vary between at least 0.2 and 1.0 m (Comparison site 'Arga' and 'Ozean', Chapter 5.3.3) within the study area. If one assumes that the model accuracy is indeed 1°C, it is sufficient to represent the spatial differences in both the thaw depth and the ground thermal regime throughout the Lena River Delta. Furthermore, it is possible to interpret the modeled distribution of ground temperatures and the processes that lead to its formation.

Warm ground temperatures mainly occur along the large river channels. In these areas, also LST is increased which could at least partly be related to warm Lena river water from the south where also the ice break-up in spring occurs earlier in the year (Käab et al. 2013). Through the warmer water, the Land Surface Temperature of even several kilometers distant grid cells may be influenced, which is taken into account in the model approach since remotely sensed LST is used as forcing data. Thus the model can represent the thermal influence of the river water.

The coldest average ground temperatures are calculated for the eastern part of the delta and towards its coastline. This could be related to a shallower snow pack in winter (see Chapter 5.2.2) which is incorporated in the forcing data. For the western half of the delta cold average ground temperatures are calculated for parts of the third stratigraphic class.

This could be due to the influence of the stratigraphic classification, assigning to these grid cells high organic upper layers and the highest ice and high organic contents for the layers below.

In addition to surface temperature and snow depth, the modeled ground temperatures are clearly influenced by ground stratigraphy. Particularly in the second model run with ERA integration, the connection between ground temperatures and ground stratigraphy becomes visible. As evident in Fig. 22 the second class is systematically warmer than the adjacent first class, which is not visible in the temperature forcing (Fig. 15). This is also confirmed by the sensitivity analysis (Chapter 5.3.4) where ground temperatures in the second class are by 1.5 to 2°C warmer than for the two other classes.

Thaw depths are strongly influenced by the stratigraphy. The lowest thaw depths are modeled for the 3rd class, which has the highest ice and organic contents with a well-insulating top layer. Medium thaw depths are modeled for the 1st class which has a little lower ice and organic contents. Sandy, organic-poor and low ice content substrate of second class lead to a faster penetration of warm temperatures in summer, causing the deepest active layer in the delta. Still, throughout the stratigraphic units some variability in thaw depths is visible that has origins other than the ground stratigraphy. An example is the northernmost edge of modeled cells of the 1st class showing shallower thaw depths which even resemble thaw depths of the 3rd class, which can most likely be explained with a shallower snow pack and colder surface temperatures towards the coastline. Towards the center and the southern part of the delta the deepest thaw depths of the 1st class are modeled. This is connected to the concurrence of early snow melt in spring, relatively warm LST values, and the fact that this area is crossed with a dense network of active river channels.

On a small scale of less than 1x1km, permafrost conditions can vary strongly, e.g. because of distribution of vegetation, snow conditions and ground conditions like topography and drainage (Zhang et al. 2014). While the model scale of $1km^2$ is too coarse to represent permafrost conditions and dynamics in heterogeneous terrain, e.g. mountain permafrost (Fiddes et al. 2013), it may be sufficient to represent permafrost temperatures in lowland tundra landscapes like the Lena River Delta. Although only seven sites were available for validation, the good agreement between measured and modeled ground temperatures and thaw depths (Chapter 5.3) suggests that the spatial variability is at least not significantly larger than the model accuracy. Additionally Langer et al. (2010) conducted a study about land surface temperature variability at a polygonal tundra site on Samoylov Island, where they showed that the differences in the LST induced by the different surface and subsurface characteristics of polygon center and polygon rim average out for averaging periods longer than the diurnal cycle.

6.2 Outlook

The results of the model validation (Chapter 5.3) indicate that CryoGrid 2 forced by remotely sensed data of surface temperature and snow depth can represent ground temperatures and thaw depths within reasonable accuracy. The presented model approach can thus be a valuable tool for the prediction of the current ground thermal regime in the climatically sensitive regions of the tundra lowlands. Therefore, it is one of the first schemes which can deliver quantitative information on the permafrost thermal state mainly based on satellite data.

The sensitivity analysis (Chapter 5.3.4) demonstrates that a realistic representation of the soil stratigraphy is a crucial prerequisite for realistic modeling, in particular of the thaw depths. In this thesis, a map of the soil stratigraphy was compiled from a number of different sources, but ultimately it is based on field mapping and observations. When the scheme should be applied to new regions, the compilation of a spatially resolved stratigraphic map (as it was done in this thesis) is a labor-intensive, but indispensable task.

Comparisons of modeled and measured mean ground temperatures show that there is a good agreement for yearly average temperatures for most validation sites in the Lena River Delta. However, the comparison of the time-resolved temperature curves suggests that frozen-ground effects of high temporal resolution, like the zero-curtain in fall and meltwater infiltration in spring (see fig. 25), are not fully represented by the model approach and the ground parameters of the soil stratification. It should be investigated if such effects are a systematic shortcoming of the model scheme, or possibly related to the spatial variability of ground properties within the 1x1 km model grid cells which cannot be represented by using only a single set of ground parameters.

As only about half of the Lena River Delta could be modeled due to the lack of snow data from GlobSnow SWE, the use of this remote sensing product is an obvious shortcoming of the model scheme. It should be checked whether alternative or additional sources of gridded data sets of snow depth could be used to make modeling of the missing parts of the Lena River Delta possible. A possibility could be to utilize the snow depths from the ERA reanalysis, although they are only available for very coarse grid cells.

The validation of the forcing data revealed too low surface temperatures of the MODIS LST product for the validation point on Samoylov Island (Chapter 5.2.1), which confirms studies from other Arctic regions (Westermann et al. 2012, Østby at al. 2014) that temporal averages of remotely sensed LST feature a significant cold-bias. For this reason the gaps in the MODIS LST time series were filled with ERA-interim 2m-air temperature, which led to much better agreement with measured surface temperatures on Samoylov

Island (Chapter 5.2.1). In addition, the CryoGrid 2 run initiated with the MODIS LST + ERA forcing data showed good agreement with measured borehole temperatures and thaw depths. If these results can be confirmed for other regions in the Arctic, the procedure of merging remotely sensed LST with reanalysis products could be an important step to achieve a more realistic monitoring of this important environmental parameter (e.g. Comiso and Parkinson 2004).

The good agreement in thaw depths suggests that the model could help to predict and estimate the release of greenhouse gases in tundra lowlands, since microbial decomposition of organic material requires the material to be unfrozen. Therefore, the thaw depth is a crucial parameter for such processes, but also the timing of thawing as delivered by CryoGrid 2 is important. The main part of the organic carbon stored in the soil is assumed to be within the first one to three meters of the ground (Strauss et al. 2012), where the model approach can deliver a reliable assessment of the ground thermal regime. Furthermore, the total amount of organic soil material must be known. In this work, the volumetric content of organic material in different stratigraphic classes has been estimated for the entire Lena River Delta and was compared to several studies. However, more work is needed to connect the emission of greenhouse gases to carbon content and thaw depth.

With the presented model scheme, a tool for the monitoring of permafrost, its thermal state and its evolution over time was developed. It may also bear the opportunity for modeling future permafrost conditions through integration of GCM data, and thus could help forecast changes in permafrost ecosystem and their carbon cycle.

7 Conclusion

In this thesis an approach for spatial modeling of the time evolution of permafrost temperatures is presented. It was implemented for the Lena River Delta in Northeast Siberia, an arctic delta with an area of about 32,000 km^2.

The model is based on the heat transfer equation, calculating the evolution of the soil temperature for every grid cell. The horizontal grid cell size is determined by the remotely sensed forcing data of MODIS Land Surface Temperature (1x1km) and the snow depth (1x1km) that was compiled from the snow water equivalent (SWE) product of GlobSnow (25x25km) and the snow extent product of MODIS (0.5x0.5km). For the reliable calculation of ground temperatures, volumetric contents of the soil constituents water/ice, mineral, organic and air are needed. Thus, a stratigraphy for the model soil domain was constructed, based on different studies on vegetation, geology, geomorphology and field book observations from many different expeditions. This stratigraphic map divides the delta into three stratigraphic classes which align to the outlines of the three main river terraces, and a typical stratigraphy is assigned to each class. The model was subsequently run for 9 years of forcing data from 2002 to 2011 and the results compared to measurements of the ground thermal regime at seven sites.

The main findings of this thesis are:

- When compared to ground measurements of surface temperature, the satellite-derived MODIS LST measurements feature a considerable cold-bias of on average 3°C, with deviations as large as 5°C for single months. If the gaps in the MODIS LST time series that occur due to cloud cover are filled with the ERA-interim 2m-air temperature product, the cold bias shrinks to -0.8 °C in the annual average and the seasonal representation improves strongly.

- The comparison of model results to ground measurements suggests an accuracy of 1°C for annual average ground temperatures and 10 cm or less for modeled thaw depths.

- A sensitivity analysis showed that the influence of the stratigraphy on ground temperatures and especially on thaw depths is strongly visible, with temperature differences up to 2 °C and differences in thaw depth of more than 50 cm between classes.

- The warmest average ground temperatures are modeled for grid cells close to the main river channels, while the coldest ground temperatures are found in the northeastern part of the delta towards the coastline.

- The lowest thaw depths are modeled for the so-called "ice complex" with ice- and organic-rich soils, as well as in areas with both low snow depths and cold average surface temperatures. The deepest thaw depths are found in areas where the stratigraphy assigns rather dry mineral soil with low ice and organic contents.

For the first time, remote sensing products were used as input for a transient permafrost model, which is capable of calculating ground temperatures at a resolution of 1km^2. However, the definition of a spatially resolved ground stratigraphy, which was based on ground observations, proved to be a crucial point for the reliable calculation of ground temperatures. The model approach is a new tool for monitoring the ground thermal state, which could be used in addition to existing ground-based monitoring in boreholes. Before application on larger scales, it should be investigated if similar model accuracies can be reached also for other permafrost areas.

8   Acknowledgements

9   References

ACIA. Impacts of a Warming Arctic: Arctic Climate Impact Assessment. Cambridge University Press, Cambridge, 2004.

ACIA. Arctic Climate Impact assessment. Scientific Report. Cambridge University Press, Cambridge, 2005.

Akhmadeeva, I., Becker, H., Friedrich, K., Wagner, D., Pfeiffer, E.-M., Quass, W. Zhurbenko, M. and Zöller, E. (1999). Investigation site 'Samoylov'. Reports on Polar and Marine Research, 315, 19-21.

Andreev, A.A., Tarasov, P.E., Schwamborn, G., Ilyashuk, B. P., Ilyashuk, E.A., Bobrov, A.A., Klimanov, V.A., Rachold, V., and Hubberten, H.-W. (2004). Holocene paleoenvironmental records from Nikolay Lake, Lena River Delta, Arctic Russia. Paleogeography, Paleoclimatology, Paleoecology, 209, 197-217.

Are, F. and Reimitz, E. (2000). An Overview of the Lena River Delta Setting: Geology, Tectonics, Geomorphology, and Hydrology. Journal of Coastal Research, 16(4), 1083-1093.

Billings, W. D. (1987). Carbon balance of Alaskan tundra and taiga ecosystems: Past, present, and future. Quaternary Science Review, 6, 165–177.

Boike, J., Wille, C. & Abnizova, A. (2008). Climatology and summer energy and water balance of polygonal tundra in the Lena River Delta, Siberia. Journal of Geophysical Research, 113, doi:10.1029/2007JG00054.

Boike, J., Kattenstroth, B., Abramova, K., Bornemann, N., Chetverova, A., Fedorova, I., Fröb, K., Grigoriev, M., Grüber, M., Kutzbach, L., Langer, M. Minke, M., Muster, S., Piel, K., Pfeiffer, E.-M., Stoof, G., Westermann, S., Wischnewski, K., Wille, C. and Hubberten, H.-W. (2013). Baseline characteristics of climate, permafrost and land cover from a new permafrost observatory in the Lena River Delta, Siberia (1998-2011). Biogeosciences, 10(3), 2105-2128.

Brown, J., Ferrians, O.J., Heginbottom, J.A., and Melnikov, E.S. (1997). Circum-Arctic map of permafrost and ground-ice conditions. Washington, DC: U.S. Geological Survey in Cooperation with the Circum-Pacific Council for Energy and Mineral Resources. Circum-Pacific Map Series CP-45, scale 1:10,000,000, 1 sheet.

Comiso, J., Parkinson, C., 2004. Satellite-observed changes in the Arctic. Physics Today 57 (8), 38–44.

Dee, D., Uppala, S., Simmons, A., Berrisford, P., Poli, P., Kobayashi, S., Andrae, U., Balmaseda, M.A., Balsamo, G., Bauer, P., Bechtold, P., Beljaars, A. C. M., van de Berg, L., Bidlot, J., Bormann, N., Delsol, C., Dragani, R., Fuentes, M., Geer, A. J., Haimberger, L., Healy, S. B., Hersbach, H., Hólm, E. V., Isaksen, L., Kållberg, P., Köhler, M., Matricardi, M., McNally, A. P., Monge-Sanz, B. M., Morcrette, J.-J., Park, B.-K., Peubey, C., de Rosnay, P., Tavolato, C., Thépaut, J.-N. and Vitart, F. (2011). The ERA-Interim reanalysis: Configuration and performance of the data assimilation system. Quarterly Journal of the Royal Meteorological Society, 137(656), 553–597.

Etzelmüller, B., Berthling, I., and Sollid, J. (2003). Aspects and concepts on the geomorphological significance of Holocene permafrost in southern Norway. Geomorphology, 52, 87–104.

Etzelmüller, B., Romstad, B., and Fjellanger, J. (2007). Automatic regional classification of topography in Norway. Norsk Geografiske Tidsskrift, 87, 167–180.

Fabrot, H., Isaksen, K., Etzelmüller, B. and Gisnås, K. (2013). Ground Thermal Regime and Permafrost Distribution under a Changing Climate in Northern Norway. Permafrost Periglacial Processes, 24, 20–38.

Federov A.N., Botulu T.A., Varlamov S.P. (1989). Permafrost Landscapes of Yakutia. 1: 2 500 000. Yakutian ASSR, GUGK (Glavnoe Upravlenie Geodezii i Kartographii USSR = Main Department of Geodezy and Cartography of USSR), Novosibirsk, 170p.

French, H (2007). The Periglacial Environment, 3rd Edition. 478 pp., John Wiley & Sons.

Gisnås, K., Etzelmüller, B., Farbrot, H., Schuler, T. V. and Westermann, S. (2013): CryoGRID 1.0: Permafrost Distribution in Norway estimated by a Spatial Numerical Model. Permafrost Periglacial Processes, 24, 2–19.

Goodrich, L. (1982). The influence of snow cover on the ground thermal regime. Canadian Geotechnical Journal, 19, 421–432.

Grigoriev, M.N. (1993). Cryomorphogenesis of the Lena River Mouth Area. Yakutsk, Russia: SB RAS, 176 p. (in Russian).

Grigoriev, M., Imaev, V., Imaeva, L., Kozmin, B., Kunitzkiy, V., Lationov, A., Mikulenko, K.I., Skrjabin, R.M., and Timirsin, K.V. (1996). Geology, seismicity and cryogenic processes in the arctic areas of Western Yakutia. Yakut Scientific Centre SD RAS, Yakutsk, 84 (in Russian).

Grigoriev, N. (1960). The temperature of permafrost in the Lena delta basin–deposit conditions and properties of the permafrost in Yakutia. Yakutsk, 2, 97-101.

Grigoriev, N. (1966). Perennially Frozen Ground of the Yakutian Maritime Zone. Moscow, USSR: Nauka, 180 p. (in Russian).

Grosse, G. Robinson, J.E., Bryant, R., Taylor, M.D., Harper, W., DeMasi, A., Kyker-Snowman, E., Veremeeva, A., Schirrmeister, L., and Harden, J., (2013). Distribution of late Pleistocene ice-rich syngenetic permafrost of the Yedoma Suite in east and central Siberia, Russia. U.S. Geological Survey Open File Report, 1078, 37p.

Gusev, A. I. (1961): Stratigraphy of Quaternary deposits of Maritime Plain. Materials of the All-Union Meeting on the study of Quaternary period. Moscow, ANSSSR, 3, 119-127 (in Russian).

Günther, F., Overduin, P.P., Sandakov, A.V., Grosse, G., and Grigoriev, M.N. (2013). Short- and long-term thermo-erosion of ice-rich permafrost coasts in the Laptev Sea region. Biogeosciences, 10(6), 4297-4318.

Hachem, S., Allard, M. and Duguay, C. (2008). A new permafrost map of Quebec-Labrador derived from near-surface temperature data of the moderate resolution imaging spectroradiometer (MODIS). Proceedings of the Ninth International Conference on Permafrost, Fairbanks, USA, 1, 591-596.

Harris et al. 1988 Harris, S., French, H., Heginbottom, J., Johnston, G., Ladanyi, B.,et al. (1988). Glossary of permafrost and related ground ice terms. Permafrost Subcommittee,

Associate Committee on Geotechnical Research, National Research Council of Canada, Ottawa.

Hoelzle, M., Mittaz, C., Etzelmüller, B., and Haeberli, W. (2001). Surface energy fluxes and distribution models of permafrost in European mountain areas: an overview of current developments. Permafrost Periglacial Processes, 12, 53–68.

Hubberten, H.-W., Wagner, D., Pfeiffer, E. M. , Boike, J., and Gukov, A.Y. (2006). The Russian-German research station Samoylov, Lena Delta - A keysite for polar research in the Siberian Arctic. Polarforschung 73, 111-116.

IPCC (2014). Climate Change 2014: Impacts, Adaptation, and Vulnerability. Part A: Global and Sectoral Aspects. Contribution of Working Group II to the Fifth Assessment Report of the Intergovernmental Panel on Climate Change. Eds. Field, C.B., V.R. Barros, D.J. Dokken, K.J. Mach, M.D. Mastrandrea, T.E. Bilir, M. Chatterjee, K.L. Ebi, Y.O. Estrada, R.C. Genova, B. Girma, E.S. Kissel, A.N. Levy, S. MacCracken, P.R. Mastrandrea, and L.L. White. Cambridge University Press, Cambridge, United Kingdom and New York, NY, USA, 1132 pp.

Kotlyakov, V. and Khromova, T. (2002). Maps of permafrost and ground ice. In: Stolbovoi V. and McCallum I., eds. Land Resources of Russia. Laxenburg, Austria. International Institute for Applied Systems Analysis and the Russian Academy of Science. CD-ROM. Distributed by the National Snow and Ice Data Center, Boulder.

Kipp & Zonen, Netherlands. Pyrgeometer. http://www.kippzonen.com/Product/16/CGR-3-Pyrgeometer#.U_i4dGNDSTk.

Langer, M., Westermann, S., and Boike, J. (2010). Spatial and temporal variations of summer surface temperatures of wet polygonal tundra in Siberia - implications for MODIS LST based permafrost monitoring. Remote Sensing of Environment, 114(9), 2059-2069.

Langer, M., Westermann, S., Heikenfeld, M., Dorn, W., and Boike, J. (2013). Satellite-based modeling of permafrost temperatures in a tundra lowland landscape. Remote Sensing of Environment, 135, 12–24.

Lawrence, D.M., and Slater, A.G. (2005). A projection of severe near-surface permafrost degradation during the 21st century, Geophysical Research Letters, 32, L24401, doi:10.1029/2005GL025080.

MDA, F. (2004). Landsat GeoCover ETM+ 2000 Edition Mosaics Tile N-52-70. USGS, Sioux Falls, South Dakota.

Minke, M., and Kirschke, S. (2007). Satellite images and ground measured reflectance spectra, thaw depth, soil moisture and vegetation type for characterizing permafrost regions. In: Boike, J., Bolshiyanov, D.Y., Grigoriev, M.N. Berichte zur Polar- und Meeresforschung. Russian-German Cooperation SYSTEM LAPTEV SEA: The Expedition LENA 2006. Bremerhaven.

Mooney, P., Mulligan, F., and Fealy, R. (2011). Comparison of ERA-40, ERA-Interim and NCEP/NCAR reanalysis data with observed surface air temperatures over Ireland. International Journal of Climatology, 31(4), 545–557.

Morgenstern A., Grosse G., and Schirrmeister L. (2008). Genetical, Morphological, and Statistical Characterization of Lakes in the Permafrost-Dominated Lena Delta. Proceedings of the Ninth International Conference on Permafrost, Fairbanks, USA, 2, 1239-1244.

71

Morgenstern, A. (2012). Thermokarst and thermal erosion: Degradation of Siberian ice-rich permafrost. Dissertation thesis, University of Potsdam.

Peter, M., (2014). Melt season dynamics in the Lena River Delta, based on remote sensing data. Course work of AGF-312 Remote Sensing of the Cryosphere, spring 2014, University Center of Svalbard, Norway.

Post, W.M., Emanuel, W.R., Zinke, P.J., and Stangenberger, A.G. (1982). Soil carbon pools and world life zones, Nature, 298, 156-159.

Rachold, V., and Grigoriev, M.N. (1999). Russian-German Cooperation System Laptev Sea 2000: The Lena Delta 1998 Expedition. Berichte zur Polarforschung (Reports on Polar Research), Bremerhaven, Alfred Wegener Institute for Polar and Marine Research, 315, 259 pp.

Riseborough, D., Shiklomanov, N., Etzelmüller, B., Gruber, S. and Marchenko, S. (2008). Recent advances in permafrost modelling. Permafrost Periglacial Processes, 19, 137–156.

Smith, M.W., and Riseborough, D.W. (1996). Permafrost monitoring and detection of climate change. Permafrost Periglacial Processes, 7, 301–309.

Romanovskii, N.N., and Hubberten, H.-W. (2001). Results of permafrost modelling of the lowlands and shelf of the Laptev Sea Region, Russia. Permafrost Periglacial Processes, 12, 191−202.

Romanovsky, V.E., Smith, S.L., and Christiansen, H.H. (2010). Permafrost thermal state in the polar Northern Hemisphere during the International Polar Year 2007-2009: a synthesis. Permafrost Periglacial Processes, 21, 106-116.

Romanovsky, V.E., Drozdov, D.S., Oberman, N.G., Malkova, G.V., Kholodov, A.L., Marchenko, S.S., Moskalenko, N.G., Sergeev, D.O., Ukraintseva, N.G., Abramov, A.A., Gilichinsky, D.A. and Vasiliev, A.A. (2010). Thermal state of permafrost in Russia. Permafrost Periglacial Processes, 21, 136–155.

Roth, K., and Boike, J., (2001). Quantifying the thermal dynamics of a permafrost site near Ny-Ålesund, Svalbard. Water Resources Research 37(12), 2901–2914.

Schirrmeister, L., Grosse, G., Schwamborn, G., Andreev, A.A., Meyer, H., Kunitsky, V.V., Kuznetsova, T.V., Dorozhkina, M.V., Pavlova, E.Y., Bobrov, A.A., and Oezen, D. (2003). Late Quaternary history of the accumulation plain north of the Chekanovsky Ridge (Lena Delta, Russia): A multidisciplinary approach. Polar Geography, 27, 277−319.

Schirrmeister, L., Grosse, G., Schnelle, M., Fuchs, M., Krbetschek, M., Ulrich, M., Kunitsky, V., Grigoriev, M., Andreev, A., Kienast, F., Meyer, H., Babiy, O., Klimova, I., Bobrov, A., Wetterich, S., Schwamborn, G. (2010). Late Quaternary paleoenvironmental records from the western Lena Delta, Arctic Siberia. Palaeogeography, Palaeoclimatology, Palaeoecology, 299, 175 – 196.

Schirrmeister, L., Grosse, G., Schnelle, M., Fuchs, M., Krbetschekd, M., Ulrich, M., Kunitsky, V., Grigoriev, M., Andreev, A., Kienast, F., Meyer, H., Babiy, O., Klimova, I., Bobrov, A., Sebastian Wetterich, S., and Schwamborn, G. (2011). Late quaternary environmental records from the western Lena Delta, Arctic Siberia. Paleogeography, Paleoclimatology, Paleoecology, 299, 175-196.

Schneider, J., Grosse, G., and Wagner, D. (2009). Land cover classification of tundra environments in the Arctic Lena Delta based on Landsat 7 ETM+ data and its application for upscaling of methane emissions. Remote Sensing of Environment, 113(2), 380-391.

Schuur, E., Bockheim, J., Canadell, J., Euskirchen, E., Field, C., Goryachkin, S., Hagemann, S., Kuhry, P., Lafleur, P., Lee, H., Mazhitova, G., Nelson, F.E., Rinke, A., Romanovsky, V.E., Shiklomanov, N., Tarnocai, C., Venevsky, S., Vogel, J.G., and Zimov, S.A. (2008). Vulnerability of permafrost carbon to climate change: Implications for the global carbon cycle. BioScience 58(8), 701–714.

Schwamborn, G., Rachold, V., and Grigoriev, M.N. (2002). Late Quaternary Sedimentation History of the Lena Delta. Quaternary International, 89, 119-134.

Schwamborn, G., Schneider, W., Grigoriev, M. N., Rachold, V., and Antonow, M. (1999). Sedimentation and environmental history of the Lena Delta. In: V. Rachold and M. N. Grigoriev, eds., Russian-German Cooperation System Laptev Sea 2000: The Lena Delta 1998 Expedition. Reports on Polar Research, 315, 94-111.

Screen, J., and Simmonds, I. (2011). Erroneous Arctic temperature trends in the ERA-40 reanalysis: A closer look. Journal of Climate, 24(10), 2620–2627.

Shiklomanov, N.I., and Nelson F.E. (2002). Active-layer mapping at regional scales: A 13-year spatial time series for the Kuparuk region, north-central Alaska. Permafrost Periglacial Processes, 13, 219–230.

SR50, Campbell Scientific, USA. http://www.campbellsci.com/sr50.

Strauss, J., Schirrmeister, L., Wetterich, S., Borchers, A., and Davydov, S.P. (2012). Grain-size properties and organic-carbon stock of Yedoma Ice Complex permafrost from the Kolyma lowland, northeastern Siberia. Global Biogeochemical Cycles, 26, GB3003, doi:10.1029/ 2011GB004104.

Ulrich, M., Grosse G., Schirrmeister L., and Chabrillat S. (2009). Spectral characterization of periglacial surfaces and geomorphological units in the Arctic Lena Delta using field spectrometry and remote sensing. Remote Sensing of Environment, 113, 1220-1235.

van Everdingen, R. (2005). Multi-language glossary of permafrost and related ground–ice terms, edited by NSIDC, Boulder, USA.

Wagner, D., Overduin, P.P., Grigoriev, M.N., Knoblauch, C., and Bolshiyanov, D.Y. (2012). Russian-German cooperation System Laptev Sea: the expedition LENA 2008. Berichte zur Polar- und Meeresforschung (Reports on polar and marine research), Bremerhaven, Alfred Wegener Institute for Polar and Marine Research, 642, 132 p.

Walker, D.A., Billings, W.D., and De Molenaar, J.G. (1997). Snow-vegetation interactions in tundra environments. In: Snow Ecology: An Interdisciplinary Examination of Snow-Covered Ecosystems, edited by H.G. Jones. Cambrigde University Press, New York.

Walker, H.J. (1998). Arctic deltas. Journal of Coastal Research, 14, 718-738.

Washburn, A. L. (1979). Geocryology: A Survey of Periglacial Processes and Environments. E. Arnold, London, 406 pp.

Westermann, S., Langer, M., and Boike, J. (2012): Systematic bias of average winter-time land surface temperatures inferred from MODIS at a site on Svalbard, Norway. Remote Sensing of Environment, 118, 162–167.

Westermann, S., Schuler, T. V., Gisnås, K., and Etzelmüller, B. (2013). Transient thermal modeling of permafrost conditions in Southern Norway, The Cryosphere, 7, 719-739.

Westermann, S., Elberling, B., Højlund Pedersen, S., Stendel, M., Hansen, B.U., and Liston, G. E. (2014). Future permafrost conditions along environmental gradients in Zackenberg, Greenland. The Cryosphere Discussion, 8, 3907-3948.

Zhang, T., Barry, R.G., Knowles, K., Heginbottom, J.A., Brown, J. (1999). Statistics and characteristics of permafrost and ground ice distribution in the Northern Hemisphere. Polar Geography 23(2), 132-154.

Zhang, T., Heginbottom, J.A., Barry, R.G., Brown, J. (2000). Further Statistics on the Distribution of Permafrost and Ground Ice in the Northern Hemisphere. Polar Geography 24(2), 126-131.

Zhang, T. 2005. Influence of the seasonal snow cover on the ground thermal regime: an overview. Reviews of Geophysics 43, 1-23.

Zhang, T., Olthof, I., Fraser, R., and Wolfe, S. A. (2014). A new approach to mapping permafrost and change incorporating uncertainties in ground conditions and climate projections. The Cryosphere, 8, 2177 – 2194.

Zimov, S.A., Voropaev, Y.V., Semiletov, I.P., Davidov, S.P., Prosiannikov, S.F., Chapin III, F.S., Chapin, M.C., Trumbore, S., Tyler, S. (1997). North Siberian lakes: A methane source fueled by Pleistocene carbon. Science, 277, 800 – 802.

Zimov, S.A., Davydov, S.P., Zimova, G.M., Davydova, A.I., Schuur, E.A.G., Dutta, K., and Chapin III, F.S. (2006). Permafrost carbon: Stock and decomposability of a globally significant carbon pool. Geophysical Research Letters, 33, L20502, doi:10.1029/2006GL027484.

Zubrzycki, S., Kutzbach, L., Pfeiffer, E.-M., and Vakhrameeva, P. (2012). Variability of Soil Organic Carbon Stocks of Different Permafrost-Affected Soils: Initial Results from a North-South Transect in Siberia. In: Proceedings of the Tenth International Conference on Permafrost 2012, Salekhard, Russia, 485-490.

Zubrzycki S., Kutzbach L., and Pfeiffer, E.-M. (2012). Böden in Permafrostgebieten der Arktis als Kohlenstoffsenke und Kohlenstoffquelle (Soils in arctic permafrost regions as carbon sink and source). Polarforschung 81(1), 33-46.

Østby, T., Schuler, T., and Westermann, S. (2014). Severe cloud contamination of MODIS Land Surface Temperatures over an Arctic ice cap, Svalbard. Remote Sensing of Environment, 142, 95-102.

Table 12: Comparison of range of thaw depths from CALM site on Samoylov Island with modeled maximum thaw depths of the corresponding grid cell for each year.

Thaw Depth Samoylov	N 72°22'10.4'',E 126°28'30.4''	
August of each year	**Measured in m (range of 150 CALM-grid points)**	**Modeled in m**
2002	0.25 - 0.6	0.48
2003	0.35 - 0.65	0.56
2004	no measurement	0.4
2005	0.42 - 0.68	0.46
2006	0.35 - 0.62	0.44
2007	0.42 - 0.7	0.5
2008	0.43 - 0.72	0.58
2009	0.25 - 0.59	0.46
2010	0.42 -0.75	0.6
2011	0.57 (max. value)	0.58
2002 - 2011	0.5	0.56

This table is the origin of Fig. 28 in Chapter 5.3.2. As part of the validation of thaw depths, the range of the CALM-Grid thaw depths from Samoylov Island, taken from 2002 to 2011, and maximum modeled thaw depths for every year are compared to each other. The CALM-Grid is a grid of 18x27.5 m with 150 measurement points for thaw depths. These measurement points all lie within a single model grid cell. The modeled thaw depths always lie within the range of yearly maximum thaw depths of the CALM site. Towards the end of the data series, the agreement seems to be better than at the beginning, which could be an effect of the short spin-up and forcing series. In the Figure, the last year is left out because the end of the thaw season in 2011 is not entirely represented in the modeling.
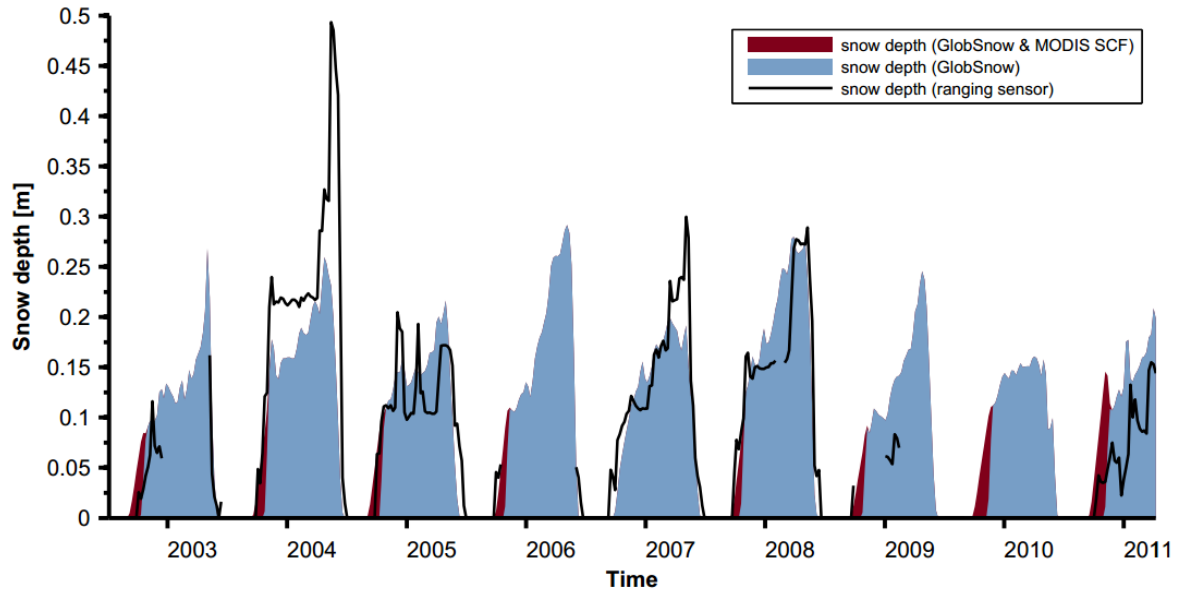
Fig. 29: Snow depth evolution of satellite measured GlobSnow SWE, here enhanced with MODIS fractional snow cover at the beginning of snow cover season, and ground measured snow depths, measured with ultra-sonic ranging sensor, from Samoylov Island. From Langer et al. (2013).

As part of the validation of forcing data this graph shows the comparison of satellite measured snow depth GlobSnow SWE, here enhanced with MODIS fractional snow cover at the beginning of snow cover season, to ground measured snow depths, measured with ultra-sonic ranging sensor on Samoylov Island. This comparison was done by Langer et al. (2013), and therefore is not featured in the result section. Here, a good agreement within 5 to 10 cm and one exception is found for the comparison of satellite and in-situ measured snow depths. The MODIS product visibly helps to represent the beginning of the snow cover more accurately which is not possible with the coarse-scaled GlobSnow product.